6-2011

Alumina-based aerogels by rapid supercritical extraction for use in green automotive catalysis

Nicholas J. Dunn
Union College - Schenectady, NY

ALUMINA-BASED AEROGELS
BY RAPID SUPERCRITICAL EXTRACTION
FOR USE IN GREEN AUTOMOTIVE CATALYSIS

By

Nicholas Jeremiah Harding Dunn

* * * * * * * * *

Submitted in partial fulfillment
of the requirements for
Honors in the Department of Chemistry

UNION COLLEGE
June, 2011

ABSTRACT

DUNN, NICHOLAS Alumina-based aerogels by rapid supercritical extraction for use in green automotive catalysis. Department of Chemistry, June 2011.

Aerogels are highly porous solids with low bulk density, high specific surface area, high thermal stability and tunable chemical composition. These properties make aerogels interesting for use as catalysts in automotive exhaust remediation. Noble metals such as platinum are currently used for this function, but are costly and harmful to the environment. Aerogels offer a potential alternative to noble metals that could reduce both the cost and environmental impact associated with catalytic converter production. Alumina and nickel-alumina aerogels have shown activity in catalyzing exhaust processing reactions. The environmental impact of the production of aerogel catalysts could be further reduced by using a rapid supercritical extraction (RSCE) technique, which reduces the time and solvent waste associated with aerogel preparation.

Alumina, nickel-alumina and copper alumina aerogels were prepared using an epoxide-assisted gelation technique followed by a solvent rinse, then RSCE on a hydraulic hot press. Samples were characterized by FTIR, XRD, SEM, EDX, nitrogen adsorption porosimetry and pycnometry.

Alumina aerogels with surface areas of up to 790 m^2/g and bulk densities as low as 0.05 g/mL were prepared, while nickel-alumina aerogels with surface areas of up to 580 m^2/g and bulk densities as low as 0.06 g/mL were produced. In the nickel-alumina and copper-alumina samples, the nickel and copper were evenly distributed throughout the material. Alumina aerogels exhibit catalytic activity for the conversion of ethanol to diethyl ether under hot press conditions. Preliminary characterization of the aerogels'

exhaust-processing ability has begun, utilizing a catalytic test bed and a simulated emissions gas blend.

Acknowledgements

I would like to thank my advisors, Professors Mary Carroll and Ann Anderson for their invaluable guidance throughout my research over the past year. They have helped to instill in me the good habits and skills that will continue to be useful throughout my research career. I would also like to thank Professor Bradford Bruno for his input on this project and his ability to ask obvious questions that would not have otherwise occurred to me. I would be remiss not to thank Professor Michael Hagerman for his assistance, both with learning how to drive the XRD , SEM and EDX attachment, and for being available to bounce crazy ideas off of. His experience in nanotechnology enabled him to help me find several key papers for this project. I would also like to recognize Professor Susan Kohler and Mark Hooker for their help using instrumentation, and for maintaining the equipment I found so useful during my research.

I would also like to extend my thanks to those people whose stay in the aerogel overlapped my own: Robin Barabasz, Lauren Brown, Suzanne Estok, Leigh Manley, Anna Mueller, Justin Rodriguez, Steve Gacin and Stephen Sanchez. They have been a pleasure to work with, and I feel that our intellectual exchanges were useful to everyone involved.

I must acknowledge Michael Bono for his foundational work in preparing alumina aerogels by rapid supercritical extraction. His work provided me with a much needed starting point for my own project.

I would also like to thank James Howard of the Machine Shop for manufacturing my stainless steel hot press molds, and Kathy Ryan for always having just the right reagent or piece of glassware.

I must acknowledge funding from the following NSF grants: NSF MRI CTS-0216153, NSF RUI CHE-0514527, NSF MRI CMMI-0722842, NSF RUI CHE-0847901, as well as from the Laudise Summer Research Fellowship and from the Union College Internal Education Fund. I would also like to acknowledge the grants that paid for the SEM: NSF MRI 0619578 and NY State Assembly RESTORE-NY.

Table Of Contents

Table of Figures

Table of Tables

Introduction

The goal of this research is to prepare and characterize alumina-based aerogel materials for use in exhaust cleaning reactions. These aerogels were prepared by Union College's patented Rapid Supercritical Extraction (RSCE) technique[1a,1b] for the purpose of reducing cost and environmental impact associated with the production of catalytic converters. Alumina, nickel-alumina and copper-alumina aerogels were produced with favorable physical properties; the characterization of catalytic effectiveness of these samples for exhaust processing is pending.

Current automotive catalytic converter technology relies on noble metals such as platinum and palladium to perform exhaust-cleaning reactions. These reactions include NO_x reduction, CO conversion and the combustion of unspent hydrocarbons, each of which reduces the environmental impact of the exhaust. Unfortunately, there is a significant negative environmental impact caused by the mining and processing of the noble metals used to perform the catalysis reactions. Aerogels have favorable properties for catalyzing gas-phase reactions such as high surface areas and tunable chemical composition. Their preparation carries less negative environmental impact than that of noble metal catalysts, especially when prepared by RSCE. Alumina and nickel alumina aerogels have even demonstrated activity in several of the reactions that are performed in modern catalytic converters.[2,3] This makes RSCE aerogels attractive as a potential replacement for the noble metals in automotive catalytic converters.

Aerogels are low-density solids that are composed of 90-99% air by volume. They have low thermal and electrical conductivities in addition to high thermal stability and tunable chemical composition, and are highly porous.[4] These properties lend them to

several different potential applications, from insulation in windows and clothing to platforms for catching cosmic dust to catalysis of a wide variety of gas phase reactions.[4] Aerogels were first discovered in the early 1930's by Kistler.[5] These first aerogels were composed of thoria and were prepared from aqueous thorium nitrate and ammonia. This synthesis took at least eleven days to yield a small amount of thoria aerogel due to the multiple lengthy solvent exchanges required before supercritical extraction of an alcohol solvent in an autoclave. Today, aerogels are typically prepared by synthesizing the porous network in solution, creating what is known as a sol gel. The solvent is then removed from the pores of the sol-gel matrix to yield an aerogel. Care must be taken to avoid capillary forces caused by the evaporation of the solvent, which will collapse the porous network of the sol gel. If these forces are not avoided, the result is a material known as a xerogel, which is approximately 60% air by volume.[4] One method for maintaining the porosity present in the sol gel while removing the solvent is to circumvent the solvent's phase transition from liquid to gas in a process known as supercritical extraction. Typically the sol gel undergoes a series of solvent exchanges until it is suspended in CO_2(l), at which point it can undergo supercritical extraction by applying sufficient heat and pressure to bypass the liquidus line of CO_2.[4] Kistler used an analogous method of supercritical extraction for his thoria aerogels, utilizing an alcohol as the solvent to be extracted rather than CO_2(l).[4]

The major disadvantages of traditional supercritical extraction methods are the time required and solvent waste generated during the solvent exchange process to get the sol gel from its reaction solvent into CO_2(l). Union College has patented an RSCE method for supercritical extraction of aerogels from their reaction solvent by utilizing a

hydraulic hot press.[1a,1b] This RSCE method is typically performed by mixing the sol-gel precursors in solution and pouring them into a steel mold. The mold is then sealed into the hot press using graphite and Kapton or stainless steel foil to ensure a complete seal and heated slowly to allow the precursor solution to gel. The temperature continues to increase, in turn increasing the pressure within the cells of the mold until the critical point of the solvent is exceeded. The hot press then reduces the restraining force on the mold to allow the supercritical solvent to vent, cools to room temperature and opens. This method can yield monolithic aerogels in less than a day and without producing a large amount of solvent waste from exchanges. An alternative application of RSCE is to allow the sol-gel to form before it is placed in the steel mold. Upon placing the sol-gel in the mold, each sample is surrounded by sufficient solvent alcohol to fill the cell, after which point the procedure is identical to the method for producing monoliths. This method produces aerogel in the shape of the sol-gel fragments that are put into the hot press and is useful for the extraction of aerogels that require chemical alteration after the sol-gel matrix has formed. The process takes less than a day from starting materials to aerogel. In practice this RSCE method reduces the cost and environmental impact associated with aerogel preparation, making them more attractive for large-scale production.

Catalytic converters are required by the EPA for all cars sold and registered in the USA.[6] The purpose of a catalytic converter is to remove harmful species from the exhaust stream by reacting them with other exhaust components to form more benign species. Important reactions performed include the reduction of NO_x, which would otherwise contribute to the formation of acid rain, the conversion of CO to CO_2 and the combustion of unspent hydrocarbons that make it into the exhaust stream.[6] Ideally, the

treated exhaust contains only CO_2, N_2 and H_2O after passing over the converter. The exhaust-cleaning reactions do not take place at low temperatures, so the converter must be kept at approximately 340ºC to operate as intended. The converter is said to have achieved its 'light off' temperature when it is successfully oxidizing 50% of the incoming hydrocarbons.[6] Catalytic converter reactions are currently performed using a thin layer of platinum, palladium or rhodium supported on a ceramic honeycomb in order to maximize the available reactive surface area in the converter. The use of these metals is the main drawback to the current catalytic converter design; the mining and processing of noble metals is damaging to the environment, which partially offsets the environmental benefits of using a converter. Additionally, the cost associated with these metals makes catalytic converters quite expensive relative to other components of the vehicle, often upwards of $1000. If aerogels can be made to act as catalysts with similar activity and specificity to these noble metal catalysts, then they will present an attractive alternative based on both financial and environmental concerns.

The porous nature of aerogels leads to a high surface area within the materials, up to 2240 m^2/g in some cases for doped carbon aerogels.[4] Surface areas of 600-800 m^2/g are considered high for alumina aerogels, and the addition of nickel decreases the expected surface area to 400-600 m^2/g.[3,7] Given this high specific surface area along with high thermal stability and tunable chemical composition, it becomes clear that aerogels have potential applications as heterogeneous catalysts for gas-phase reactions. These heterogeneous systems benefit greatly from a high surface area on the catalyst which increases the number of exposed active sites for reaction, thereby increasing the efficiency of the reaction with respect to the gas flow.

As a result of their favorable properties as catalysts or catalytic supports, aerogels have already been put to use in a variety of gas-phase catalytic applications (Table 1-1).

Table 1-1: Some Catalytically Active Aerogels Described in the Literature

Aerogel	**Reaction**	**Reactant**	**Product**	**Ref**
Ni-Al_2O_3	conversion	CO and NO	CO_2 and N_2	3
Ni-Al_2O_3	isomerization	1-butene	*cis/trans*-2-butene	3
Ni-Al_2O_3	reformation	CO_2, CH_4	CO, H_2 (syngas)	9
Al_2O_3	dehydration	CH_3OH	CH_3OCH_3	10
Al_2O_3	reduction	NO, NH_3	N_2, H_2O	2
ZrO_2	isomerization and hydrogrenation	*n*-butene	*cis*/*trans*-2-butene / butane	11
V_2O_5-TiO_2	selective oxidation	H_2S	S and $(NH_4)_2S_2O_3$	12
V_2O_5-TiO_2	reduction	NO, NH_3	N_2, H_2O	13
mixed Mg/Fe oxide	reduction	NO, NH_3	N_2, H_2O	14
Cu-SiO_2	reduction	NO, C_3H_8, C_3H_6	N_2, H_2O	15
V-SiO_2	reduction	NO, C_3H_8, C_3H_6	N_2, H_2O	15
Fe oxide-Cr_2O_3-Al_2O_3	reduction	NO, NH_3	N_2, H_2O	16
Rh-TiO_2-SiO_2	hydrogenation	benzene	cyclohexane	17
CuO	oxidation and photo-oxidation	2-nitrophenyl	CO_2, H_2O, HNO_3, unknown	18
ZrO_2-SO_4^{2-}	isomerization (superacid)	*n*-butane	isobutane	19
SiO_2-Al_2O_3	oligomerization	propene	polypropylene	8
SiO_2	cracking	cumene	benzene, propane	20
Pd-Al_2O_3	automotive	CO, NO, O_2	CO_2, N_2	21
Pd- SiO_2-Al_2O_3	combustion	CH_4	CO_2, H_2O	22
$CoFe_2O_4$	hydrolysis	4-nitrophenyl phosphate	4-nitrophenol	4

Silica and alumina aerogels are most often used as supports for catalytically active species, although both materials have also demonstrated catalytic activity on their own.

Silica aerogels reduced under a hydrogen stream have been used for cracking cumene to generate benzene and propane,[8] while copper and vanadium supported on silica aerogels have demonstrated reductive activity for the conversion of NO to N_2 and H_2O.[15] Mixed silica and alumina aerogels have been used for the oligomerization of propene to polypropylene, and mixed titania-silica aerogels supporting rhodium have been used in the hydrogenation of benzene.[17] Silica aerogels have also demonstrated acidic catalytic behavior for the isomerization of 1-butene when combined with zirconia[7] and niobia.[8] Vanadia-titania aerogels have been used for the selective oxidation of H_2S to afford S and $(NH_4)_2S_2O_3$,[12] as well as for the reduction of NO in the presence of NH_3 to form N_2 and H_2O.[13]

Other less standard aerogel compositions have been used in catalytic applications as well. Zirconia aerogels have shown both isomerization and dehydrogenation activity on *n*-butene to form *cis*/*trans*-2-butene and butane respectively.[11] Zirconia-sulfate aerogels have shown superacid properties in the isomerization of *n*-butane[10] that would potentially make them useful as fuel cracking catalysts. Copper oxide aerogels have been used in the photo-oxidation of 2-nitrophenyl to produce CO_2, H_2O and HNO_3 in a model reaction for the processing of environmental pollutants.[14] Mixed-phase iron oxide / chromia / alumina aerogels have demonstrated NO reducing activity in the presence of NH_3,[16] as have mixed-phase magnesium oxide / iron oxide aerogels.[18] Copper silica aerogels have been used for the reduction of NO in the presence of hydrocarbons,[15] a reaction of interest to the automotive industry because it doesn't use NH_3 as the reductant. Since copper is the catalytically active species in this material, it could potentially be

transplanted to another supporting material and utilized in concert with other exhaust-cleaning species.

Nickel-alumina aerogels have proven particularly versatile as catalysts, and have shown activity for CO and NO conversion, hydrogenation, methanization, isomerization and dehydrogenation.[3] Alumina aerogels have been used in alcohol dehydration to form ethers,[10] and alumina is known to catalyze the formation of ethers when heated.[23] Unmodified alumina aerogels have also been used as NO_x reduction catalysts with some success.[2] The CO conversion and NO_x reduction reactions over alumina and nickel alumina are of particular interest because these reactions are performed in automotive catalytic converters with similar catalysts, making alumina and nickel alumina aerogels attractive compositional choices for aerogels as noble metal replacements. By modifying the preparation methods for these aerogels to use RSCE rather than traditional extraction methods it may be possible to provide the basis for green, inexpensive catalytic converters.

References

[1a] Gauthier, B.M., Bakrania, S.D., Anderson, A.M. and Carroll, M.K. 2004. "Simplified Technique for Fabricating Aerogel Monoliths Using Fast Supercritical Extraction." *J. Non-Cryst. Solids* 350, 238

[1b] Gauthier, B. M., Anderson, A. M., Bakrania, S., Mahony, M.K. and Bucinell, R.B., "Method and device for fabricating aerogels and aerogel monoliths obtained thereby." U.S. Patent 7,384,988. 10 June 2008

[2] Hirashima, H., Kojima, C., Imai, H., 1997. "Application of Alumina Aerogels as Catalysts." *J. Sol-Gel Sci, Technol*. 8, 843-846

[3] Krompiec, S., Mrowiec-Bialon, J., Skutil, K., Dukowitz, A., Pajak, L., Jarzebski, A.B., 2004. "Nickel-alumina composite aerogel catalysts with a high nickel load: a novel fast sol-gel synthesis procedure and screening of catalytic properties." *J. Non-Cryst. Solids* 315, 297-303

[4] Pierre, A. and Pajonk, G. 2002. "Chemistry of aerogels and their applications." *Chem. Rev.* 102, 4243-4265

[5] Kistler, S. S. 1932. "Coherent Expanded Aerogels." *J. Phys. Chem.* 36, 52-64

[6] Brandt, E.P, Wang, Y. and Grizzle, J.W. 1999. "Dynamic modeling of a three-way catalyst for SI engine exhaust emission control." *IEEE Contr. Syst. T.* 20, 1-9

[7] Baumann, T.F., Gash, A.E., Chinn, S.C., Sawvel, A.M., Maxwell, R.S. and Satcher, J.H. 2005. "Synthesis of high surface-are alumina aerogels without the use of alkoxide precursors." *Chem. Mater.* 17, 395-401

[8] Willey, R.J., Teichner, S.J., Pajonk, G.M., 1992. "Reactivity of SiO_2 aerogel activated by hydrogen spillover for the hydrogenation of ethylene and the cracking of cumene." *J. Molec. Catal.* 77, 201-219

[9] Hao, Z.; Zhu, Q.; Lei, Z.; Li, H. 2008. "CH_4-CO_2 reforming over Ni/Al_2O_3 aerogel catalysts in a fluidized bed reactor." *Powder Technol.* 182, 474-479

[10] Tleimat-Manzaji, R.; Bianchi, D.; Pajonk, G.M. 1993. "CH_3OH conversion in dimethyl ether on porous and amorphous alumina gels of high surface area." *React. Kinet. Catal. Lett.*, 51, 29-37

[11] Pajonk, G.M.; El Tanany, A. 1992. "Isomerization and hydrogenation of butene-1 on a zirconia aerogel catalyst." *React. Catal. Lett.* 47, 167-175

[12] Kim, M.I., Park, D.W., Park, S.W., Yang, X., Choi, J.S., Suh, D.J., 2006. “Selective oxidation of hydrogen sulfide containing excess water and ammonia over vanadia-titania aerogel catalysts.” *Catal. Today* 111, 212-216

[13] Kang, M.; Choi, J.; Kim, Y.T.; Park, E.U.; Shin, C.B.; Suh, D.J.; Yie, J.E. 2009. "Effects of preparation methods for V_2O_5-TiO_2 aerogel catalysts on the selective catalytic reduction of NO with NH_3." *Korean J. Chem Eng.* 26, 884-889

[14] Willey, R.J.; Kotur, E.; Kehoe, J.; Busca, G., in *Sol-Gel Processing and Applications*, Attia Y., Ed., Springer. 1994. "Preparation and evaluation of mixed magnesium oxide-iron oxide aerogels for the selective catalytic reduction of nitric oxide." 351-361

[15] Owens, L.; Tillotson, T.M.; Hair, L.M. 1995. "Characterization of vanadium / silica and copper / silica aerogel catalysts." *J. Non-Cryst. Solids* 186 177-183

[16] Willey, R.J.; Lai, H.; Peri, J.B. 1991. "Investigation of Iron Oxide-Chromia-Alumina Aerogels for the Selective Catalytic Reduction of Nitric Oxide by Ammonia." *J. Catal.* 130, 319-331

[17] Cauqui, M.A.; Calvino, J.J.; Cifredo, G.; Esquivas, L.; Rodríguez-Izquierdo, J.M. 1992. "Preparation of rhodium catalysts dispersed on TiO_2-SiO_2 aerogels." *J. Non-Cryst. Solids* 147-148, 758-763

[18] Bandara, J.; Kiwi, J.; Pulgarin, C.; Pajonk, G. 1996. "Catalytic oxidation and photo-oxidation of nitrophenols by strong oxidants generated in situ via CuO-aerogel." *J. Molec. Catal. A* 111, 333-339

[19] Ward, D.A.; Ko, E.I.; 1994. "One-step synthesis and characterization of zirconia-sulfate aerogels as solid superacids." *J. Catal.* 150, 18-33

[20] Rouanet, S.; Willey, R.; Peri, J., in *Sol-Gel Processing and Applications*, Attia, Y., Ed., Springer, 2004. "Investigation and characterization of silica-alumina aerogels." 285-293

[21] Hoang-Van, C.; Pommier, B.; Harivololona, R.; Pichat, P. 1992. "Alumina-based aerogel as carriers for automotive palladium catalysts." *J. of Non-Cryst. Solids* 145, 250-254

[22] Mizumisha, Y.; Hori, M. 1995. "Alumina-silica aerogel catalysts prepared by two supercritical drying methods for methane combustion." *J. Mater. Sci.* 30, 1551-1555

[23] Jain, J. R.; Pillai, C. N. 1967. "Catalytic Dehydration of Alcohols over Alumina: Mechanism of Ether Formation." *J. Catal.* 9, 322-330

Aerogel Synthesis and Physical Characterization Experimental

Aerogel Synthesis

Aerogels were synthesized by the epoxide-assisted method,[3] using propylene oxide as the epoxide and alcohols for solvents. $AlCl_3 \cdot 6H_2O$ (Fisher, >99% purity) was used as the aluminum source for all of the synthesized aerogels, while $Ni(NO_3)_2 \cdot 6H_2O$ (Fisher, >99% purity) was used as the nickel source for aerogels incorporating nickel. $Cu(NO_3) \cdot 3H_2O$ (Acros Organics, 99%) was used as the copper source for aerogels incorporating copper. Nickel and copper were incorporated both directly (during the initial gelation of the sol-gel) and indirectly (during a solvent exchange), as described below. Solvent alcohols employed included methanol (Fisher, ≥99.8%) ethanol (Fisher, 97% and Pharmco-AAPER, 200 proof) and 2-propanol (Fisher, ≥99.5%). Propylene oxide (Sigma Aldrich, 99%) was used as the gelation agent for all recipes. Table 2-1 contains a complete list of recipes used.

Sol Gel Preparation

First, the amount of $AlCl_3 \cdot 6H_2O$ prescribed in Table 2-1 was dissolved in 20 mL of solvent-grade ethanol. $AlCl_3 \cdot 6H_2O$ is not particularly soluble in ethanol, so magnetic stirring and/or sonication was applied until no particulates were visible. Once the precursor salt had dissolved, 9.48 mL propylene oxide was added to the mixture with mechanical stirring of the solution using a magnetic stir bar. Gelation occurred in fewer than 3 min after the addition of the propylene oxide. The sol gel was allowed to set overnight before undergoing a solvent rinse with ethanol.

Table 2-1: Recipes for the Preparation of Sol Gels

Recipe	Solvent	Alcohol (mL)	Water (mL)	$AlCl_3$ •$6H_2O$ (g)	$Ni(NO_3)_2$ •$6H_2O$ (g)	$Cu(NO_3)_2$ •$3H_2O$ (g)	Metal addition method	Propylene Oxide (mL)
Ep1	EtOH	20	-	2.96	-	-	n/a	9.48
Ep2W	EtOH/H_2O	10	10	2.96	-	-	n/a	9.48
Ep3	EtOH	20	-	2.06	-	-	n/a	9.48
NEp1	EtOH	20	-	2.86	0.11	-	direct	9.48
NEp2	EtOH	20	-	2.26	0.843	-	direct	9.48
NEp3W	EtOH/H_2O	10	10	2.86	0.11	-	direct	9.48
NEp4W	EtOH/H_2O	10	10	2.26	0.843	-	direct	9.48
Nimp	EtOH	20	-	2.96	0.915	-	solvent exchange	9.48
IsEp1	2-propanol	20	-	2.96	-	-	n/a	9.48
IsEp2W	2-propanol /H_2O	10	10	2.96	-	-	n/a	9.48
NIsEp1	2-propanol	20	-	2.26	0.843	-	direct	9.48
NIsImp	2-propanol	20	-	2.96	0.915	-	solvent exchange	9.48
MeEp1	MeOH	20	-	2.96	-	-	n/a	9.48
MeNEp2	MeOH	20	-	2.26	0.843	-	direct	9.48
MeNImp	MeOH	20	-	2.96	0.915	-	solvent exchange	9.48
CEp1	EtOH	20	-	2.26		0.0700	direct	9.48
CEp2	EtOH	20	-	2.26	-	0.700	direct	9.48
CImp-D	EtOH	2-	-	2.96	-	0.0091	solvent exchange	9.48
CImp	EtOH	20	-	2.96	-	0.0910	solvent exchange	9.48

This table contains the recipes used to prepare sol gels. Those recipes which contain a 'W' in their name were prepared in a water-containing solvent, while those with 'Imp' in their name had a secondary metal besides aluminum added through solvent exchange. In all other recipes I directly added all of the metal salts to the precursor solution prior to gelation.

The solvent rinse was preceded by breaking up the sol-gel matrix by gentle agitation with a glass stirring rod in order to facilitate a faster exchange. The reaction solvent was then poured off, and a volume of 20 mL of absolute ethanol was added to the broken sol-gel. The sol gel was allowed to sit overnight in its original 50-mL beaker

covered with parafilm. The entire gelation and rinsing procedure can also be performed in less than a day by utilizing two 2-h solvent rinses after allowing the sol gel to set for 3 h. This decrease in processing time appeared to have little effect on the properties of the resulting aerogels.

The directions above were also used to prepare recipes with other alcohols, substituting either methanol or 2-propanol for ethanol at every step. Changing the solvent alcohol did not change the gelation time noticeably. For recipes incorporating water as part of the solvent, a 50/50 (v/v) water/alcohol solution was used to perform the initial gelation reaction, and 20 mL of the alcohol was used for the solvent exchange.

To prepare a nickel-alumina or copper-alumina sol gel by the direct addition method, the amount of $AlCl_3 \bullet 6H_2O$ was reduced to keep the total number of moles of metal in the solution consistent with the alumina recipe Ep1. $Ni(NO_3)_2 \bullet 6H_2O$ or $Cu(NO_3)_2 \bullet 3H_2O$ was added to the beaker at the same time as the $AlCl_3 \bullet 6H_2O$, prior to gelation. The specific amounts of each reagent are given in Table 2-1.

To prepare a nickel-alumina or copper-alumina sol gel by solvent impregnation, $Ni(NO_3)_2 \bullet 6H_2O$ or $Cu(NO_3)_2 \bullet 3H_2O$ was added to the exchange solvent. Since the addition of these metal salts occurs post-gelation, the amount of $AlCl_3 \bullet 6H_2O$ used to prepare the sol gel was the same as for an alumina sol gel. Specific amounts for each reagent can be found in Table 2-1.

Solvent Extraction

After the alcohol rinse, the sol gel was ready to undergo RSCE. The sol-gel fragments were divided evenly between the cells of a stainless steel mold, with the

remaining space in each cell filled with the solvent alcohol from the preparation recipe. The mold measured 12.6 x 12.6 x 1.8 cm (length by width by height), and had four circular wells measuring 4 cm in diameter and 1.5 cm in depth. The mold was then placed on a hydraulic hot press and sealed with graphite and a thin sheet of non-stick material to prevent the graphite from sticking to the mold. Both Kapton and stainless steel foil were used for this purpose, but Kapton displayed some reactivity with an unknown component of the precursor mixture under supercritical conditions and was not used after the stainless steel foil became available. Table 2-2 below contains a list of the programs used for RSCE on the hot press. 2-Propanol has a lower critical temperature (235 ºC) than methanol (240 ºC) or ethanol (241 ºC), and so programs for extracting it were able to use a lower maximum temperature.

For all programs the restraining force was applied at a rate of 890 kN/min and released at a rate of 4.4 kN/min. Due to the fast heating rate in the rapid program, a dwell time of 30 min was set after the heating step to allow the contents of the mold to come to thermal equilibrium at the desired temperature.

Table 2-2: Hot Press Program Parameters

Program	Solvent	High Temp (ºC)	Heating Rate (ºC/min)	Cooling Rate (ºC/min)	Restraining Force (kN)
6A	EtOH	268	1.1	1.1	170
6B	EtOH	251	1.1	1.1	170
6C	EtOH	251	3.3	1.1	170
6D	EtOH	251	2.2	1.1	170
6E	EtOH	246	2.2	1.1	170
6F	EtOH	248	2.2	1.1	170
6F*45	EtOH	248	2.2	1.1	200
6F*45 Is	2-propanol	246	2.2	1.1	200
6F*45B	EtOH/MeOH	248	2.2	2.2	200
6F*45B Is	2-propanol	246	2.2	2.2	200
Rapid	EtOH	248	22	22	200

Preparation of Aerogel-Coated Cordierite

Aerogel layers were mounted onto cordierite matrices by placing pieces of cordierite in the precursor solution and allowing the sol gel to form around them. These samples were subjected to a passive solvent rinse by soaking in absolute ethanol in a beaker covered by parafilm overnight without agitation or stirring. The coated cordierite was then transferred to a cell in the stainless mold to undergo supercritical extraction in the same way as any other aerogel sample.

Aerogel Characterization

After RSCE, samples were subjected to analysis by Fourier transform infrared spectroscopy (FTIR), powder x-ray diffraction (XRD), bulk density measurements, pycnometry, surface area analysis (BET), pore size distribution (BJH) and scanning electron microscopy (SEM). All measurements were taken on samples that had been finely ground using a mortar and pestle.

FTIR spectroscopy was performed on a Mattson Galaxy 6020 FTIR Spectrophotometer using the Smart Orbit ATR attachment with 32 scans and a resolution of 4 cm^{-1} for both the background (ambient air) and the sample scans.

XRD patterns were obtained from a Phillips PW-1840 X-ray diffraction instrument over a 2θ range of 10-100º with a Co radiation source. The patterns were taken at 0.6º 2θ/min with a voltage of 45 keV and a current of 35 mA. Samples were mounted on aluminum sample plates as pressed powders.

Bulk density measurements were taken by comparing mass and volume measurements in disposable polystyrene cuvettes. The cuvettes were each massed before

and after the addition of the ground aerogel. The internal cross-sectional area of the cuvettes was known to be 1.00 cm x 1.00 cm, so the height of the sample could be measured and the volume occupied could be calculated from these dimensions. This method is expected to underestimate the density of a given sample due to non-ideal packing of the pieces of aerogel within the cuvette.

Skeletal density measurements of finely ground samples were made on a Micromeritics AccuPyc 2020 gas pycnometer, and are the result of taking repeated measurements until the last four trials agreed with each other within 0.1 g/mL. The average of these four trials was reported for each sample. The number of measurements taken varied due to different amounts of adsorbed material on the aerogel samples.

BET and BJH measurements were taken on two Micromeritics instruments: the Tristar 3000 porosimeter and the ASAP 2010 porisimeter, with nitrogen used as the adsorption gas and liquid nitrogen used to maintain the temperature of the samples during testing for both instruments. For the Tristar 3000 instrument, samples were degassed in the attached Micromeritics Smartprep degassing unit for 2 h at 90 ºC and 10 h at 200 ºC with constant nitrogen flow. For the ASAP, samples were degassed under a vacuum of 0.67 Pa while being heated to 90 ºC for 2 h and 200 ºC for 5 h.

SEM images of the samples were taken on a Zeiss EVO50 Scanning Electron Microscope at varying magnifications. A working distance of 7.0-8.5 mm combined with an accelerating voltage of 6.50-8.00 keV was best for high-magnification imaging of alumina, nickel-alumina and copper-alumina aerogels. A Bruker Quantax 200 EDX system with a Peltier-cooled XFlash silicon drift detector attachment was used in conjunction with the SEM to gain energy dispersive x-ray (EDX) data. A working

distance of 8.5-9.0 mm with an accelerating voltage of 10.00-15.00 keV was optimal for obtaining EDX spectra.

Results and Discussion: Physical Characterization

IR Spectroscopy

IR spectroscopy did not show any significant difference between alumina and nickel-alumina RSCE aerogels of different recipes and processing conditions. The observable peaks appear to be primarily due to bond vibrations that were common to each aerogel, most likely those from the alumina matrix. There were no significant differences between spectra of aerogels prepared from methanol- and ethanol-based recipes, and alumina aerogels were very similar to nickel-alumina aerogels. Aerogels prepared using 2-propanol were too hydrophilic to give high quality IR spectra. They have a broad O-H bending peak centered around 3300 cm^{-1} that also appears around 1650 cm^{-1}, obscuring much of the interesting detail.

The three figures on the following pages contain representative FTIR spectra of alumina (Fig. 3-1), nickel-alumina (Fig 3-2) and copper-alumina (Fig 3-3) aerogels prepared using ethanol. Both the alumina and nickel-alumina spectra (Figs. 3-1 and 3-2) share several peaks in common, particularly those at 2970 cm^{-1}, 1385 cm^{-1} and 610 cm^{-1}. These are all due to vibrations involving aluminum, with the 2970 cm^{-1} peak representing the asymmetric AlO-H stretch within a boehmite crystalline phase and the 1385 cm^{-1} peak representing an O-H vibration in boehmite.[1] These peaks are not identical to those found in the literature, with 3092 cm^{-1} given for the asymmetric AlO-H stretch and 1340 cm^{-1} given for the O-H vibration.[1] Subtle changes in coordination geometry and interaction strength can substantially change the frequency and intensity of these peaks,[1] which may account for the shift of the AlO-H stretch from 2970 cm^{-1} in alumina to 3092 cm^{-1} in nickel-alumina.

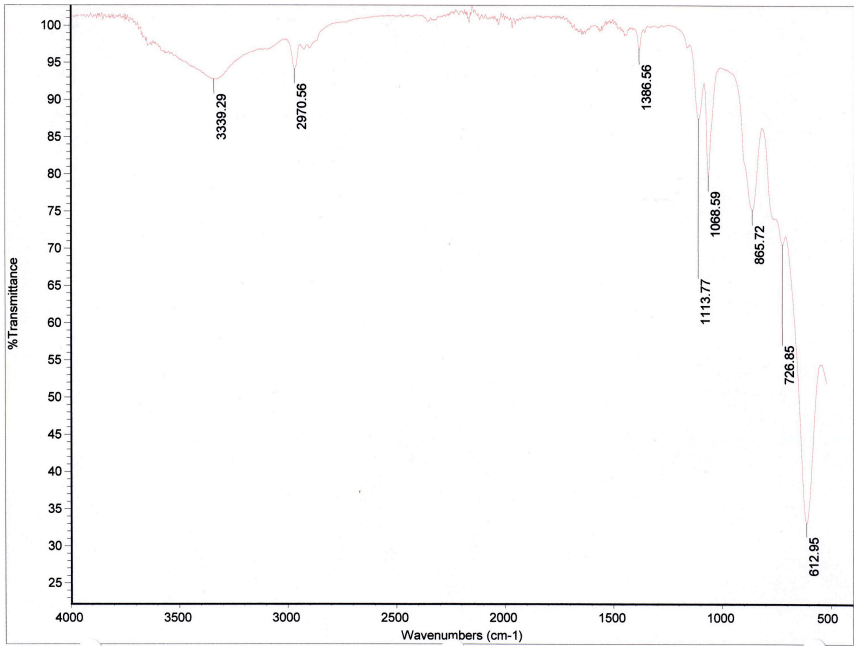

Figure 3-1: The IR spectrum for Ep1 7/18/10, a representative alumina aerogel sample. The spectrum is the result of averaging 32 scans taken at 4 cm^{-1} resolution.

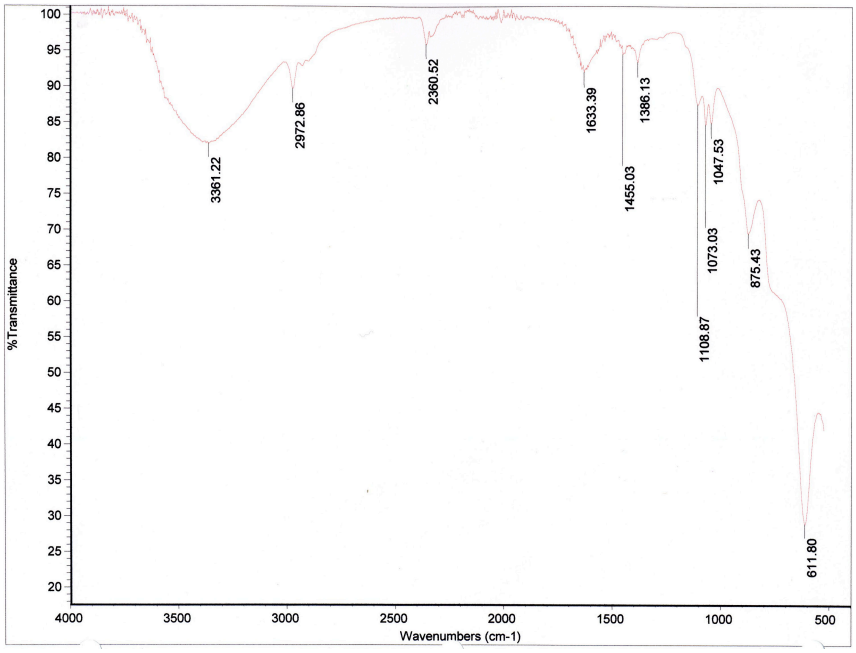

Figure 3-2: IR spectrum for NEp2 7/14/10, a representative nickel-alumina aerogel sample. The spectrum is the result of averaging 32 scans taken at 4 cm^{-1} resolution.

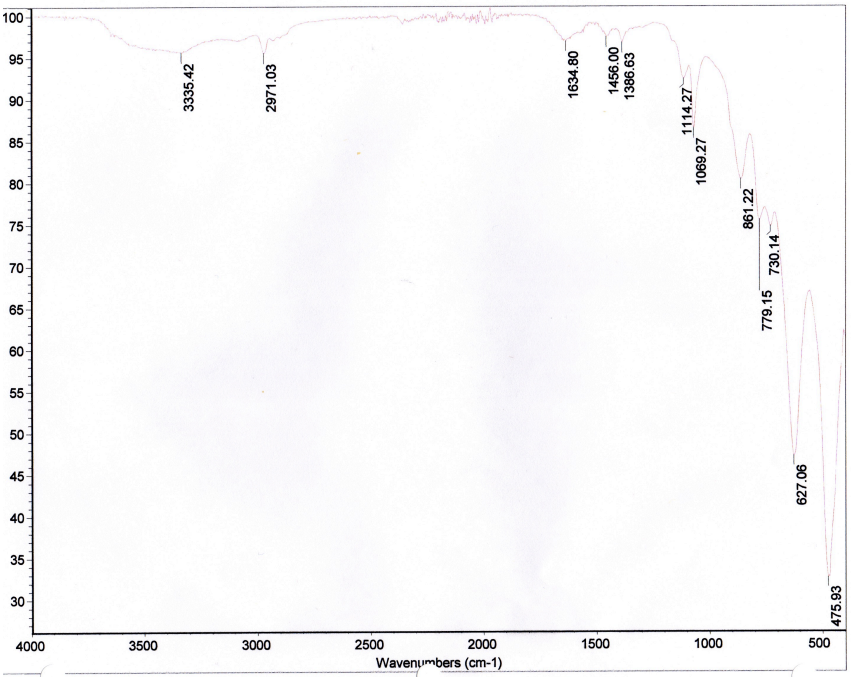

Figure 3-3: IR spectrum for CEp2 1/18/11, a representative copper-alumina aerogel sample. The spectrum is the result of averaging 32 scans taken at 4 cm^{-1} resolution.

The specific interaction leading to this shift is not known at this time. The peak at 610 cm^{-1} indicates the presence of octahedrally coordinated aluminum.[2]

Other peaks present in the unmodified alumina aerogel (Fig. 3-1) correspond closely with literature values,[1] with the peaks at 1110 cm^{-1} and 1070 cm^{-1} corresponding to asymmetric and symmetric stretching of AlO-H groups in boehmite phases. It is unclear at this time to what the remainder of the peaks in the fingerprint region correspond.

The spectrum for the nickel-alumina aerogel (Fig. 3-2) is very similar to the unmodified alumina spectra (Fig.3-1). Again, peaks are found at 1110 cm^{-1} and 1070 cm^{-1}, but they are much less intense than in the samples that do not contain nickel or copper. Additionally, there is a peak directly adjacent to these two at 1050 cm^{-1} that was not present in the alumina spectrum. This peak may be due to an interaction with nickel

splitting one of the stretching peaks or a separate nickel-related peak coincidentally falling at a similar frequency.

Copper-alumina aerogels have IR spectra which are similar to those of unmodified alumina aerogels with two main exceptions. The peak at 610 cm^{-1} in alumina shifted to 627 cm^{-1} when in copper-alumina samples, suggesting that there is some limited interaction between the copper and alumina coordination spheres. Additionally, the shoulder on the peak at 730 cm^{-1} in the alumina aerogel is better resolved as a peak at 780 cm^{-1}, indicating a change in relative peak intensity between the two samples. This difference is subtle, but may indicate another interaction between the copper and aluminum centers. Other copper-related peaks are not observed in this spectrum (Fig. 3-3) because copper is too heavy for its peaks to be seen in the mid-IR range.

Powder X-Ray Diffraction

The presence of boehmite phases within the RSCE aerogels is supported by the XRD patterns for these samples which show Bragg peaks indicative of boehmite as well as γ-alumina.[3] Figure 3-4 below shows a typical diffraction pattern for an alumina aerogel. The sharp, intense peaks at d = 2.36, 2.04, 1.44, 1.23 and 1.17 are due to the aluminum sample holder and provide an indication of the quality of the peaks due to the aerogel material. The peak at d = 1.84 might correspond to γ-alumina, which does not typically show up in materials prepared at relatively low temperatures, such as these aerogels experienced during processing.[4] This sharp and intense peak would seem to be a significant crystalline phase within the material, but the particular phase responsible has not yet been confidently identified. The remaining broad peaks at 2θ = 17º, 32º, 44º, 47º

and 86º are due to a boehmite crystalline phase present in the material.[3] The boehmite peaks are broad because of the small size of the individual boehmite crystals within the aerogel. A slightly different distribution of boehmite peaks can be seen in aerogels prepared using methanol, with additional peaks appearing at 2θ = 41º and 73º, as seen in Figure 3-5. Boehmite formation is known to be sensitive to changes in solution conditions[3] so this is not unexpected, although more diverse boehmite distributions might have been expected among the ethanol, ethanol/water and isopropyl alcohol samples.

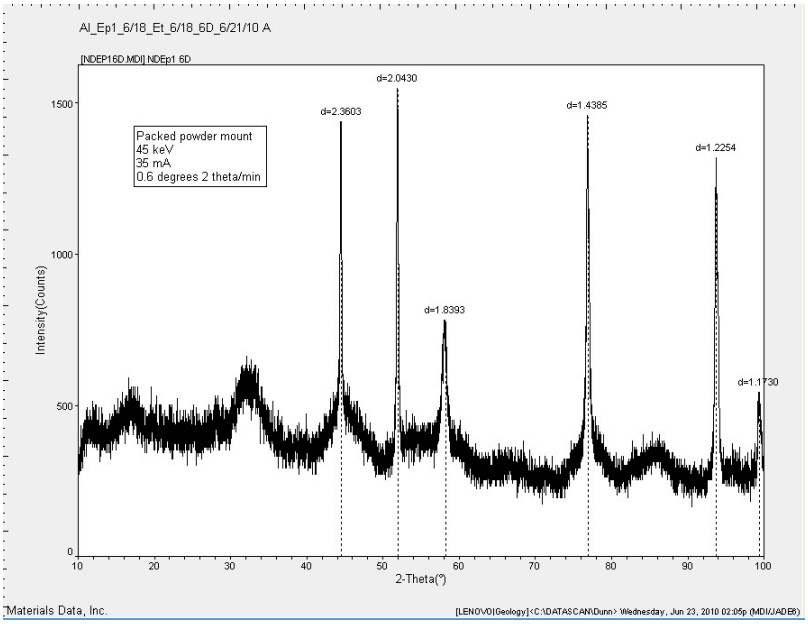

Figure 3-4: An XRD pattern of Ep1 6/21/10 A, a representative alumina aerogel. The sample was scanned as a packed powder mount from 10-100º 2θ at 0.6º/min, with the x-ray source operating at 45 keV and 35 mA. The sharp peaks at d = 2.36, 2.04, 1.44, 1.23 and 1.17 are due to the aluminum sample holder rather than to the aerogel sample.

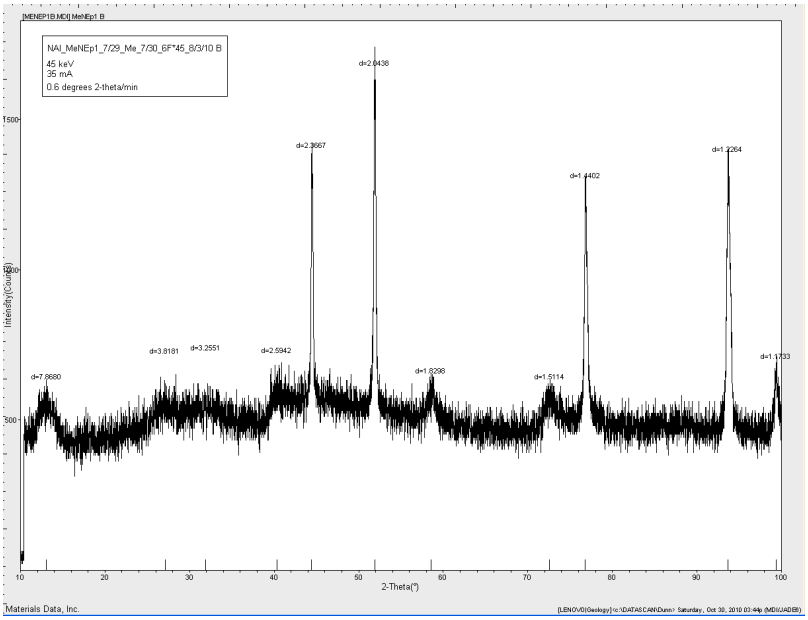

Figure 3-5: An XRD pattern of MeNEp2 8/3/10, a nickel-alumina aerogel prepared using methanol in which nickel was incorporated by direct addition. The sample was scanned as a packed powder mount from 10-100º 2θ at 0.6º/min, with the x-ray source operating at 45 keV and 35 mA. The sharp peaks at d = 2.36, 2.04, 1.44, 1.23 and 1.17 are due to the aluminum sample holder rather than to the aerogel sample.

The Bragg peaks seen in the unmodified alumina aerogel are common to all of the aerogel recipes invesigated by XRD, though there is some variability in peak intensity and breadth. In particular, those aerogels that contained water as a component of their reaction solvent showed sharper, more intense peaks as can be seen in Figure 3-6. Peak intensity and sharpness also increased for those aerogels that did not undergo a solvent rinse before extraction. This indicates that lack of a solvent exchange lent itself to more and larger crystalline domains within the material. More amorphous samples were also seen, especially in nickel-alumina aerogels (as shown in Figure 3-7, below). In the absence of water in the precursor mixture, aerogels prepared using 2-propanol were fully amorphous. When water was present in the precursor mixture, aerogels prepared using 2-propanol had similar crystallinity to samples in which ethanol and water were used in the precursor mixture.

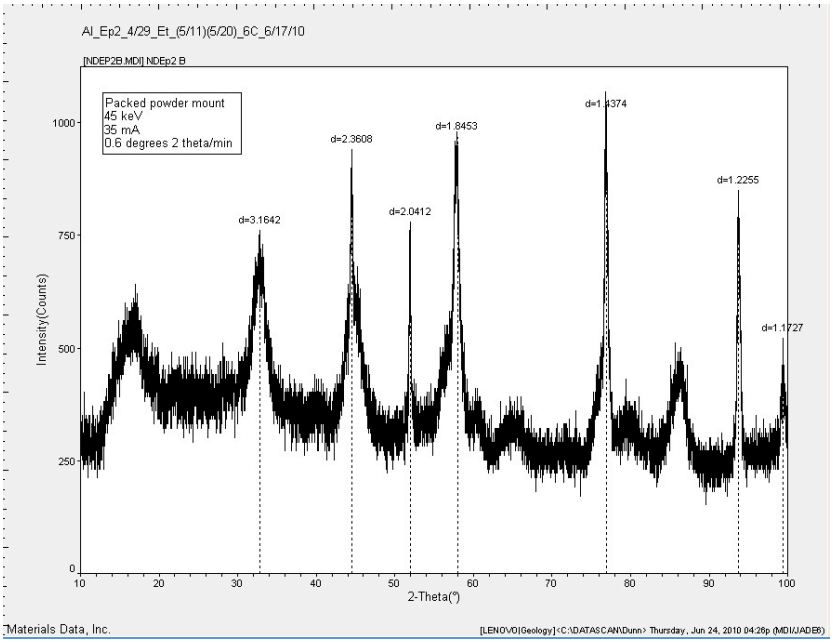

Figure 3-6: An XRD pattern of Ep2 6/17/10, an unmodified alumina aerogel that used a 50/50 water/EtOH reaction solvent. The sample was scanned as a packed powder mount from 10-100º 2θ at 0.6º/min, with the x-ray source operating at 45 keV and 35 mA. The sharp peaks at d = 2.36, 2.04, 1.44, 1.23 and 1.17 are due to the aluminum sample holder rather than to the aerogel sample.

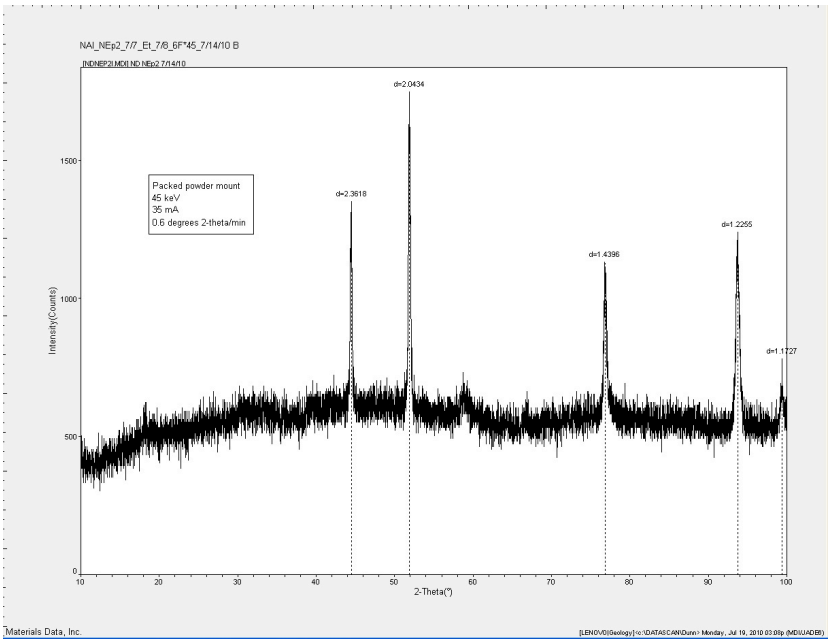

Figure 3-7: An XRD pattern of NEp2 7/14/10, a nickel-alumina aerogel which incorporated nickel by direct addition. The sample was scanned as a packed powder mount from 10-100º 2θ at 0.6º/min, with the x-ray source operating at 45 keV and 35 mA. The sharp peaks at d = 2.36, 2.04, 1.44, 1.23 and 1.17 are due to the aluminum sample holder rather than to the aerogel sample.

XRD patterns for high copper-content direct addition (Fig - 3-8, CEp2) and solvent impregnation (Figure 3-9, CImp) copper alumina aerogels can be seen below. These two diffraction patterns contain a pair of Bragg peaks characteristic of CuO at $2\theta = 50.7^{\circ}$ and $2\theta = 55.6^{\circ}$.[5] This implies the formation of copper oxides in the material, which were observed as a red powder around the aerogel samples after RSCE. There is also a Bragg peak at $2\theta = 33^{\circ}$ in both samples, a peak at $2\theta = 19.8^{\circ}$ in the solvent impregnation sample and a peak at $2\theta = 66.4^{\circ}$ present in the direct addition sample. These peaks are possibly associated with other CuO_x species or with copper metal, but they exist outside of the range over which the diffraction of these materials is studied. The low copper-content versions of these recipes did not contain any peaks that were not present in an unmodified alumina sample.

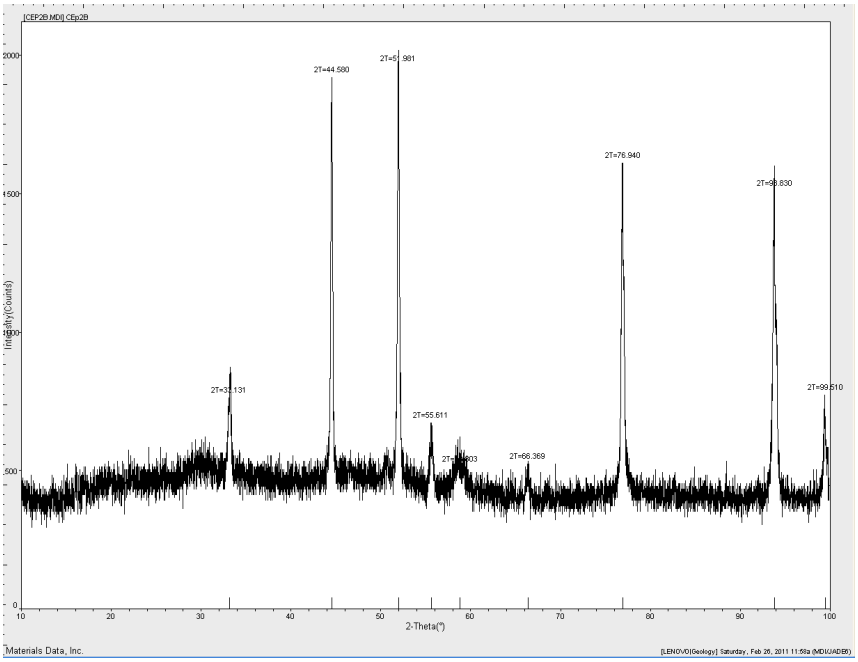

Figure 3-8: An XRD pattern of CEp2, a copper-alumina aerogel which incorporated copper by direct addition. The sample was scanned as a packed powder mount from 10-100º 2θ at 0.6º/min, with the x-ray source operating at 45 keV and 35 mA. The sharp peaks at d = 2.36, 2.04, 1.44, 1.23 and 1.17 are due to the aluminum sample holder rather than to the aerogel sample.

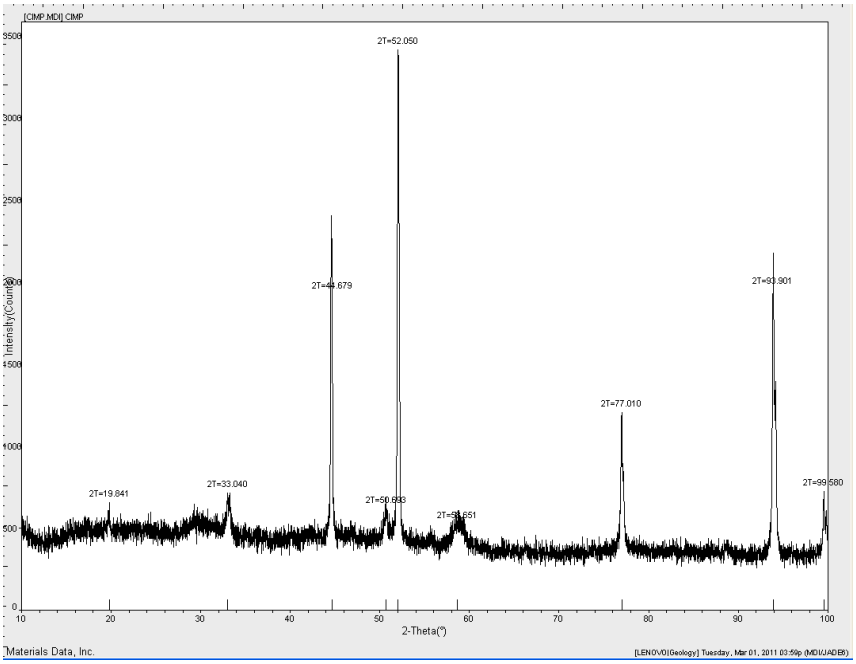

Figure 3-9: An XRD pattern of CImp, a copper-alumina aerogel which incorporated copper by solvent impregnation. The sample was scanned as a packed powder mount from 10-100º 2θ at 0.6º/min, with the x-ray source operating at 45 keV and 35 mA. The sharp peaks at d = 2.36, 2.04, 1.44, 1.23 and 1.17 are due to the aluminum sample holder rather than to the aerogel sample.

Textural Qualities

The surface areas and bulk densities of RSCE alumina and nickel-alumina aerogels, seen in Table 3-1 below, are within the range of values seen in the literature,[6,7] with obvious differences arising from composition and extraction conditions. In particular, the nickel alumina samples prepared by solvent impregnation (NImp) is within the 400-600 m^2/g range, specified as a high surface area range for the material by Krompiec et al.[8] Additionally, alumina aerogels which were prepared using methanol had surface areas towards the top of the 600-800 range observed by Baumann et al.[3]

The uncertainty in the surface area was calculated by aggregating the uncertainty from the BET measurement (u_{SA}) with the uncertainty in the mass measurement due to the extent of degassing (u_{mass}). The following formula was used to calculate uncertainty:

$$u_{net} = \sqrt{\left(\frac{u_{SA}}{SA}\right)^2 + \left(\frac{u_{mass}}{mass}\right)^2}$$

A similar equation was used for the uncertainty in the bulk density measurement, aggregating the uncertainty in the volume measurement with that of the mass measurement. In the first two entries of the table it can be seen that a single solvent rinse substantially increases the surface area and decreases the density of the resulting aerogel significantly. Also, the use of water as a reaction solvent component decreased the surface area markedly while increasing the bulk density. This can be seen by comparing the results for the water-based Ep2 batch with those for any Ep1 batch that underwent a solvent exchange. Water had the same effect on nickel-alumina aerogels, as seen in the comparison between NEp1 and NEp2 (which did not incorporate water) with NEp3W and NEp4W (which did include water). This corresponds with the increase in crystallinity seen in the XRD results, suggesting that the aerogels lose surface area as they lose some of their amorphous character. For all solvents except 2-propanol, the addition of nickel either by direct addition or by solvent exchange decreased the surface area of the aerogel sample, with direct addition of nickel resulting in all cases in a lower surface area than solvent impregnation. Nickel-alumina aerogels had similar properties regardless of the solvent used, whereas alumina aerogels varied dramatically in quality. Those alumina aerogels prepared with methanol gave the highest surface area; those prepared with 2-propanol the lowest. This suggests that the solvent alcohol has a subtle effect on formation of the sol-gel network that is counteracted by the addition of nickel.

Additionally, an aging effect appears as surface area measurements are repeated. Older aerogel samples seem to lose surface area over time at ambient conditions, which is not an encouraging result.

Table 3-1: BET Surface Area and Bulk Density of RSCE Aerogel Samples

Sample ID	BET Surface Area (m^2/g)	Bulk Density (g/mL)	Solvent	Secondary Metal and Addition Method
Ep1 UX	160 ± 6	0.23 ± 0.03	ethanol	n/a
Ep1 XC	320 ± 10	0.16 ± 0.02	ethanol	n/a
Ep1	630 ± 30	0.07 ± 0.01	ethanol	n/a
Ep2W	250 ± 10	0.28 ± 0.03	ethanol/water	n/a
Ep3	330 ± 20	0.21 ± 0.03	ethanol	n/a
NEp1	490 ± 20	0.11 ± 0.01	ethanol	dilute Ni, direct
NEp2	460 ± 20	0.09 ± 0.01	ethanol	Ni, direct
NEp3W	310 ± 20	0.14 ± 0.02	ethanol/water	dilute Ni, direct
NEp4W	160 ± 5	0.40 ± 0.05	ethanol/water	Ni, direct
NImp1	580 ± 10	0.10 ± 0.01	ethanol	Ni, impregnation
IsEp1	240 ± 10	0.19 ± 0.02	2-propanol	n/a
IsNEp1	480 ± 20	0.11 ± 0.01	2-propanol	Ni, direct
IsNImp1	500 ± 40	0.05 ± 0.01	2-propanol	Ni, impregnation
MeEp1	790 ± 50	0.05 ± 0.01	ethanol	n/a
MeNEp1	480 ± 20	0.06 ± 0.01	ethanol	n/a
MeNImp1	550 ± 20	0.13 ± 0.01	ethanol	n/a
NImp Rapid	280 ± 10	0.05 ± 0.02	ethanol	Ni, impregnation
NEp2 Rapid	230 ± 10	0.11 ± 0.01	ethanol	Ni, direct
CEp1	-	0.043 ± 0.04	ethanol	dilute Cu, direct
CEp2	-	0.13 ± 0.02	ethanol	Cu, direct
CImp	-	0.12 ± 0.01	ethanol	Cu, impregnation
CImp-D	-	0.046 ± 0.005	ethanol	dilute Cu, impregnation

These samples also take much longer to equilibrate in the pycnometer than when they were fresh, suggesting the presence of adsorbed species that are being displaced by the helium. IR spectra of these sample show some growth of broad -OH stretching peak relative to spectra taken on freshly prepared samples.

Skeletal densities for the aerogel samples can be seen below in Table 3-2. The accepted range for the skeletal density of alumina is between 2.5 and 4.0 g/mL, depending on the particular connectivity of the solid as well as its level of hydration. Within the aerogels prepared using ethanol, the skeletal density is lower for the nickel-

alumina aerogels than for alumina aerogels, suggesting a possible influence on backbone structure or on adsorbed water on the surface of the material. In the only recipe incorporating water as part of the reaction solvent tested so far, Ep2W, the skeletal density is above 3 g/mL, suggesting a high level of hydration. Although IsNImp1 did not use water in its reaction solvent, it also has a high skeletal density, which might be attributable to either waters of hydration or isopropyl alcohol tightly adsorbed to the material's surface. Both of the nickel-alumina aerogels that were prepared using ethanol, NEp2 and NImp1, had a lower skeletal density than the equivalent alumina aerogel Ep1. The aerogel MeEp1, prepared using methanol as its reaction solvent, also had a lower skeletal density than Ep1, which was prepared using ethanol. More samples must be tested before general conclusions can be made from these variations.

Pore size distributions found by the BJH method for RSCE alumina and nickel-alumina aerogels are similar to those seen in the literature,[7] concentrated in the 10-100 nm range, indicating the successful preparation of a nanoporous material. The primary pore diameters of all samples tested can be seen in Table 3-3.

The use of water as part of the reaction solvent leads to a narrower distribution of pore diameters than the use of anhydrous ethanol for both alumina and nickel alumina aerogels, but there is a tradeoff in surface area that occurs with the water/alcohol aerogels. For instance, Ep1 has a specific surface area of 630 ± 30 m^2/g and a primary pore diameter of 30 nm with a distribution width of 60 nm, whereas Ep2W has a specific surface area of 250 ± 10 m^2/g and a primary pore diameter of 25 nm with a distribution width of 30 nm. The only processing difference between these two samples is that for Ep1 I used anhydrous ethanol as the solvent and Ep2W had a 50/50 water/ethanol

reaction solvent.

Additionally, the distribution profile is not changed significantly by the inclusion of nickel, as can be seen below in Figures 3-10 and 3-11. Despite the increased amount of noise present in the distribution for the nickel-alumina sample, both materials display a peak in the 30-40 nm range surrounded by similar topography. This indicates that the nickel is not severely compromising the porosity of the alumina support, thereby preserving the desired surface area for catalysis applications.

Table 3-2: Skeletal Densities of RSCE Aerogel Samples

Sample	Skeletal Density (g/mL)	Solvent	Secondary Metal and Addition Method
Ep1	2.75	ethanol	n/a
Ep2W	3.12	ethanol/water	n/a
Ep3	3.15	ethanol	n/a
NEp1	2.58	ethanol	dilute Ni, direct
NEp2	2.609	ethanol	Ni, direct
NEp3W	2.916	ethanol/water	dilute Ni, direct
NEp4W	3.16	ethanol/water	Ni, direct
NImp1	2.581	ethanol	Ni, impregnation
IsEp1	4.32	2-propanol	n/a
IsNEp1	3.42	2-propanol	Ni, direct
IsNImp1	3.72	2-propanol	Ni, impregnation
MeEp1	2.56	ethanol	n/a
MeNEp1	2.625	ethanol	n/a
MeImp	2.477	ethanol	n/a
NImp Rapid	3.271	ethanol	Ni, impregnation
NEp2 Rapid	3.107	ethanol	Ni, direct
CEp1	2.78	ethanol	dilute Cu, direct
CEp2	3.06	ethanol	Cu, direct
CImp	3.22	ethanol	Cu, impregnation
CImp-D	3.09	ethanol	dilute Cu, impregnation

Table 3-3: Primary Pore Diameters of RSCE Aerogel Samples

Sample	Primary Pore Diameter (nm)	Solvent	Secondary Metal and Addition Method
Ep1	30	ethanol	n/a
Ep2W	25	ethanol/water	n/a
Ep3	30	ethanol	n/a
NEp1	20	ethanol	dilute Ni, direct
NEp2	30	ethanol	Ni, direct
NEp3W	40	ethanol/water	dilute Ni, direct
NEp4W	20	ethanol/water	Ni, direct
NImp1	20	ethanol	Ni, impregnation
IsEp1	30	2-propanol	n/a
IsNEp1	30	2-propanol	Ni, direct
IsNImp1	30	2-propanol	Ni, impregnation
MeEp1	30	ethanol	n/a
MeNEp1	30	ethanol	n/a
MeImp	25	ethanol	n/a
NImp Rapid	20	ethanol	Ni, impregnation
NEp2 Rapid	70	ethanol	Ni, direct
CuEp1	-	ethanol	dilute Cu, direct
CuEp2	-	ethanol	Cu, direct
CuImp	-	ethanol	Cu, impregnation
CuImp-D	-	ethanol	dilute Cu, impregnation

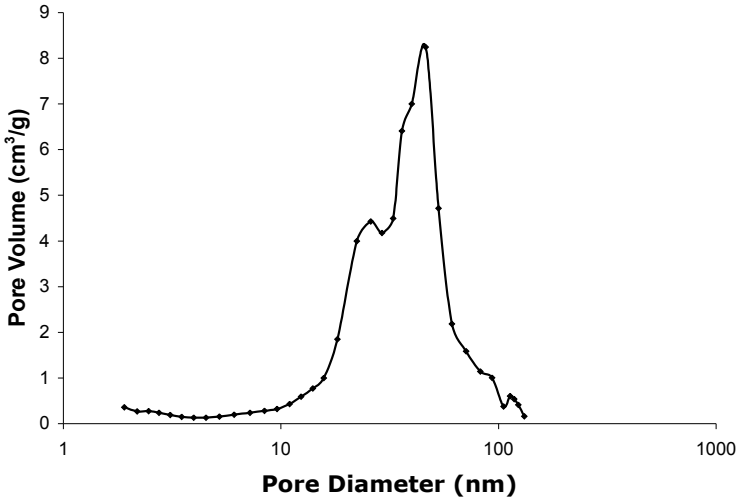

Figure 3-10: BJH pore size distribution for Ep1 4/30/10, a representative alumina aerogel. The sample was degassed for 2 h at 90 ºC and 10 h at 200 ºC under a constant nitrogen flow. Please note that the x-axis scale is logarithmic.

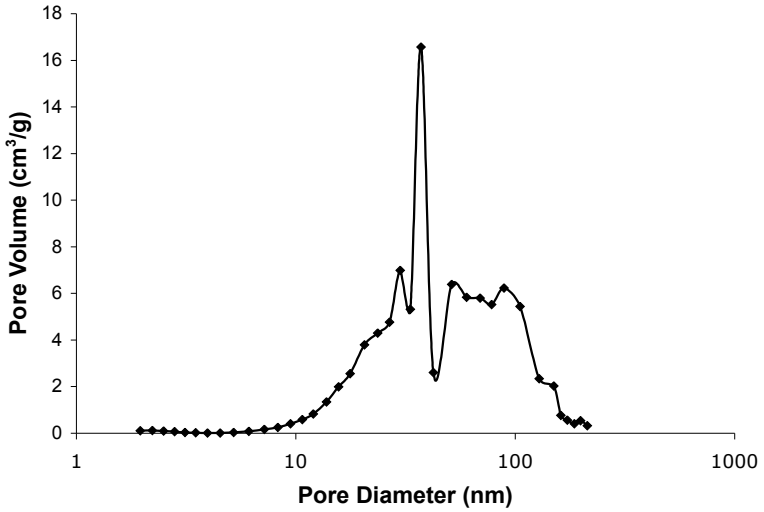

Figure 3-11: BJH pore size distribution for NEp2 6/15/10, a nickel-alumina aerogel with nickel added directly. The sample was degassed for 2 h at 90 ºC and 10 h at 200 ºC under a constant nitrogen flow. Please note that the x-axis scale is logarithmic.

Scanning Electron Microscopy

The BJH pore size distribution is corroborated by SEM images of the aerogel samples that show porosity in the 10-100 nm range. Figure 3-12 contains high magnification SEM images of four different aerogel samples that have visible nanoporosity at the magnifications used. Of the four samples in Figure 3-12, (c) stands out as having significantly different surface appearance, with its visible pores being significantly smaller than those of other samples. This may be because (c) is a nickel-alumina aerogel prepared by solvent impregnation. The nickel could have deposited within the pores of the alumina aerogel. If so, this would explain the reduced BET surface area of solvent-impregnated nickel-alumina aerogels compared to their unmodified alumina counterparts. The other three samples in Figure 3-12 show porosities that are similar to each other, consistent with the pore distributions collected for the alumina and direct addition nickel-alumina aerogels.

In order to make the aerogel material resistant to gas flow conditions in an exhaust line a coating of aerogel material was applied to a cordierite ceramic honeycomb. Cordierite is used currently as a support for the heavy metal catalysts in catalytic converters, so binding aerogels to cordierite would allow their catalytic properties to be more easily compared to those of conventional catalysts. Figure 3-13 below shows uncoated cordierite at several magnifications, and at each level the cordierite is distinct from aerogel material, most notably in (d) where it can be seen that the ceramic has a globular rather than a porous structure.

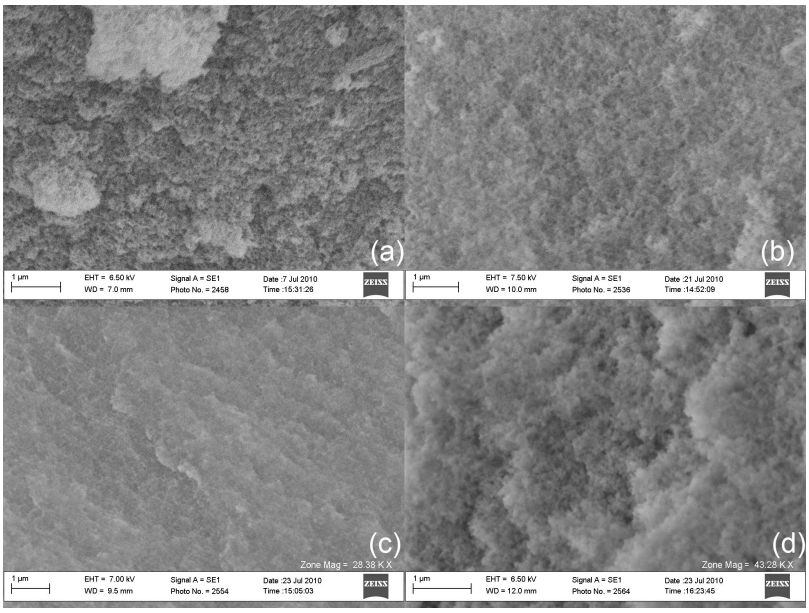

Figure 3-12 - SEM images of: **a)** Ep1 5/26/10, an alumina aerogel **b)** NEp2 7/14/10, a nickel-alumina aerogel with the nickel added directly **c)** NImp1 7/14/10, a nickel-alumina aerogel with the nickel added by solvent exchange **d)** NIsEp1 7/19/10, a nickel-alumina aerogel with 2-propanol as the reaction solvent and the nickel added directly. Images are at 30000-45000x magnification, and a 1-µm scale bar is present in the lower left of each image.

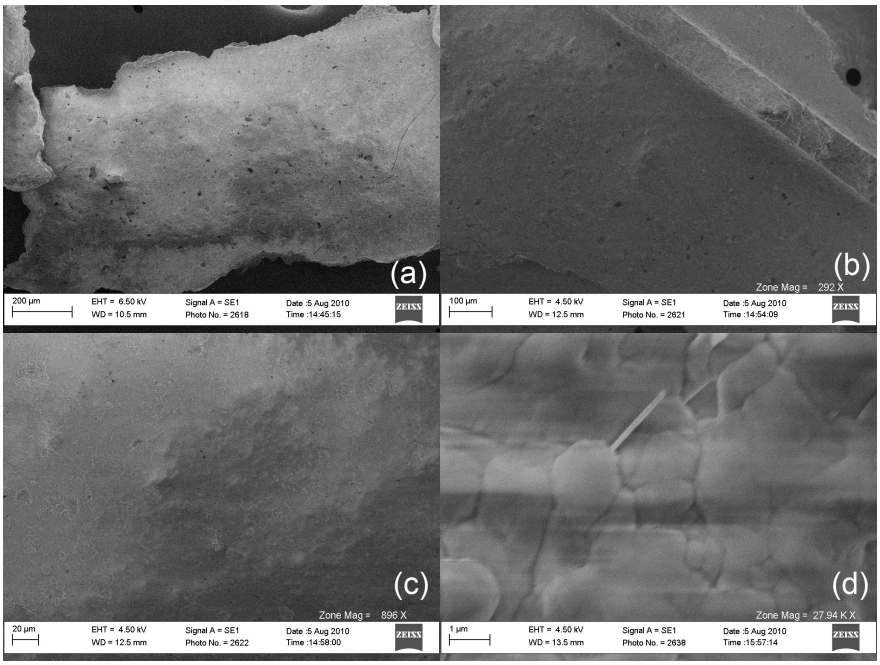

Figure 3-13 - SEM images of unmodified cordierite at increasing magnifications. 3-11a is presented at 100x magnification. All other magnifications can be seen in the lower right of the image.

By contrast, in the images in Figure 3-14 it can be seen that there is significant silica aerogel material coating the ceramic surface. Layering is apparent even at the low magnification in (a), and zooming in on an apparently smooth area shows that it is porous in nature, clearly indicating the presence of aerogel material on the surface. This material survived significant agitation during the collection and mounting process, suggesting that it is firmly fixed to the ceramic. Figure 3-15 shows the results of coating a cordierite sample with alumina aerogel. The aerogel distribution is more uneven than for the silica coating, with some cordierite material visible through gaps in the alumina aerogel material. Such gaps are not observed in the silica aerogel coating, so the the thinnest parts of the alumina coating appear to be thinner than those of the silica. It should be noted that this particular alumina aerogel did not undergo a solvent exchange because of time constraints on using the hydraulic hot press.

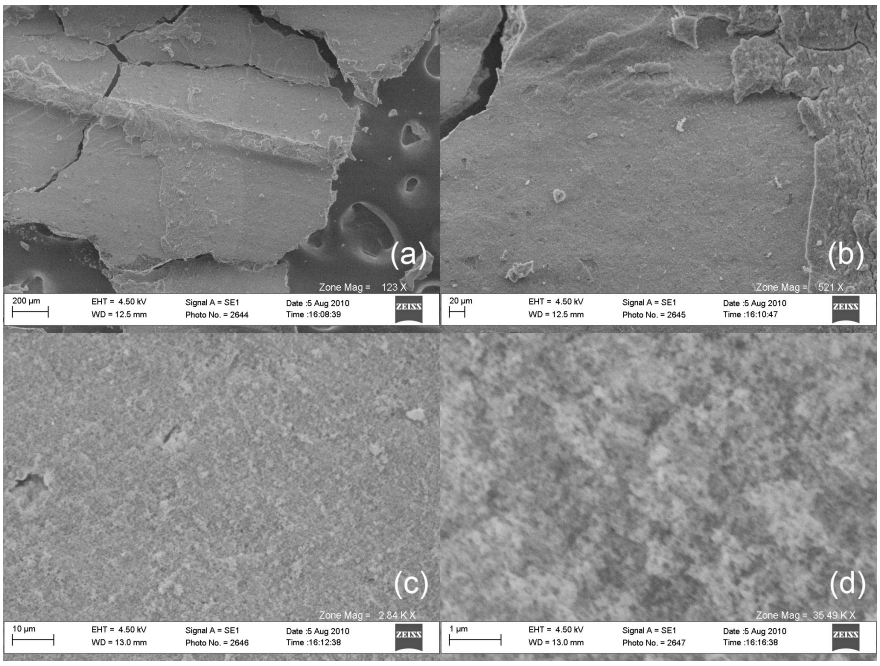

Figure 3-15 - SEM images of silica-coated cordierite at increasing magnifications from **a)** to **d)**.

Figure 3-16 shows SEM images of an alumina-coated cordierite sample that underwent a solvent exchange, this sample demonstrates a similar morphology to that seen in Figure 3-15. The nickel-alumina coating that can be seen in Figure 3-17 has a distinct surface texture from the unmodified alumina samples, showing a higher prevalence of fine texturing on the surface, which is not evident at low magnifications. It should be noted that a significant amount of aerogel material fell away from the ceramic during the preparation of both the alumina and silica-coated cordierite samples. This material seems to have been occupying the channels within the cordierite rather than binding to the walls, and its removal did not appear to correlate with a loss of aerogel coating on the cordierite surface. SEM images of cordierite samples indicated that we can coat the surface of a cordierite ceramic with several types of aerogel material: silica, alumina and nickel-alumina.

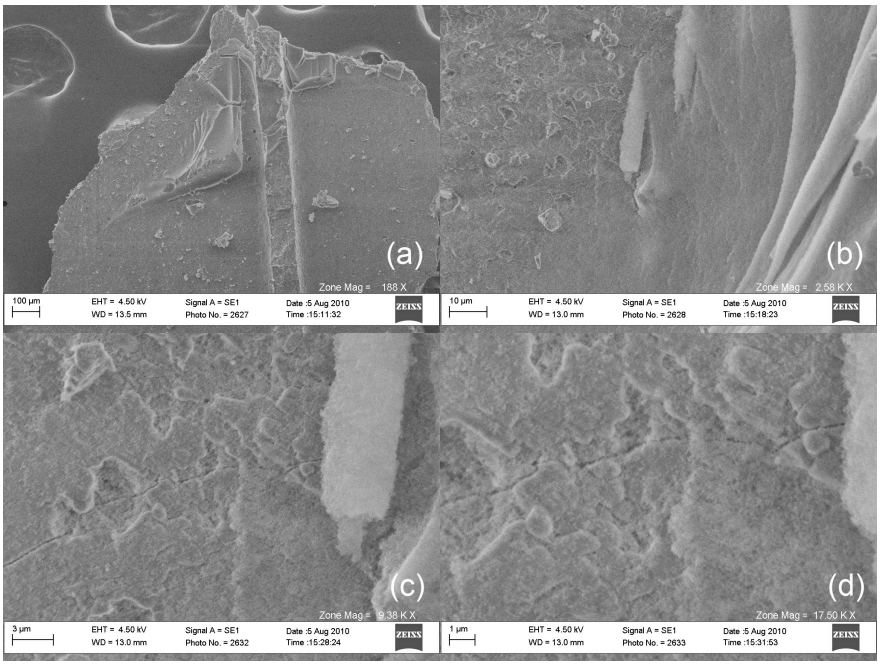

Figure 3-15 - SEM images of alumina-coated cordierite for which the aerogel did not undergo a solvent exchange (UX Ep1). Images presented at increasing magnifications from **a)** to **d)**.

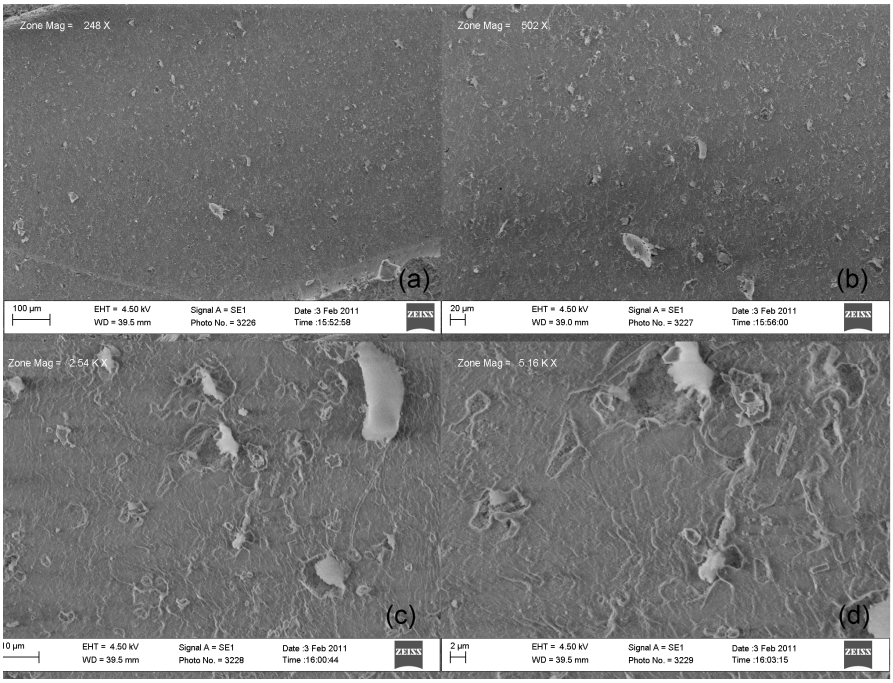

Figure 3-16 - SEM images of alumina-coated cordierite for which the aerogel underwent a typical solvent exchange (Ep1). Images presented at increasing magnifications from **a)** to **d)**.

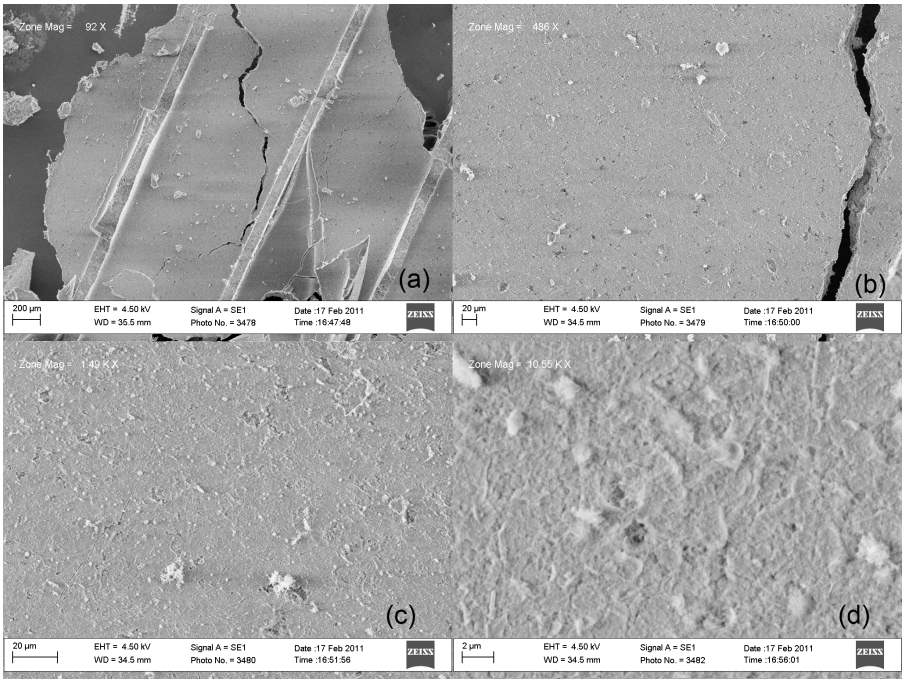

Figure 3-17 - SEM images of nickel-alumina-coated cordierite incorporating nickel through direct addition (NEp2). Images presented at increasing magnifications from **a)** to **d)**.

Additional work should be done in characterizing the cordierite-coating capabilities of the variety of aerogel recipes tested. Aerogels that have less appealing physical properties such as lower surface areas or unfavorable pore size distributions may prove to bind to the ceramic better than more appealing materials. Different coating methods should also be explored, such as dip coating or employing rotation of the cordierite on an axis perpendicular to the pores in the cordierite material to ensure uniform coating thickness.

Energy Dispersive X-Ray Spectroscopy

Energy dispersive x-ray (EDX) spectroscopy was employed to determine the elemental compositions of aerogel samples, as well as the spatial distribution of these elements throughout the material. The spectrum of a linear section of an unaltered

alumina aerogel (Ep1) can be seen in Figure 3-18, which shows strong peaks for both aluminum and oxygen, as expected for an alumina material. Peaks are also present at lower magnitudes for iron and silicon, suggesting that there may be some contamination of the sample occurring either during gelation or during processing in the stainless steel mold. There is also a significant chlorine peak, suggesting that not all of the byproducts or starting materials are being removed over the course of the single solvent exchange.

EDX line spectra for nickel-alumina aerogels show similar chorine and silicon peaks, but are apparently free of iron contamination (Figs. 3-19 and 3-20), and demonstrate the expected aluminum, oxygen and nickel peaks.

Copper-alumina aerogels prepared by direct addition show the same iron and chlorine contamination as the nickel-alumina aerogels, but do not demonstrate silicon contamination to the same extent as the nickel-alumina samples. The spectra for both the low copper-content sample (CEp1, Fig. 21) and the high copper-content sample (CEp2, Fig. 22) contain the expected aluminum and oxygen peaks, as well as significant copper peaks. Similarly, copper-alumina aerogels prepared by solvent impregnation show iron and chlorine contamination, but no significant silicon peaks are present in either the low copper-content material (CImp-D, Fig. 3-23) or the high copper-content material (CImp, 3-24). As anticipated, the low copper-content samples (Fig. 22 and Fig. 24) have less intense copper peaks. These lower intensity copper peaks correspond to a lower iron peak intensity. This suggests that copper might be involved in the mechanism of iron uptake by the aerogel material.

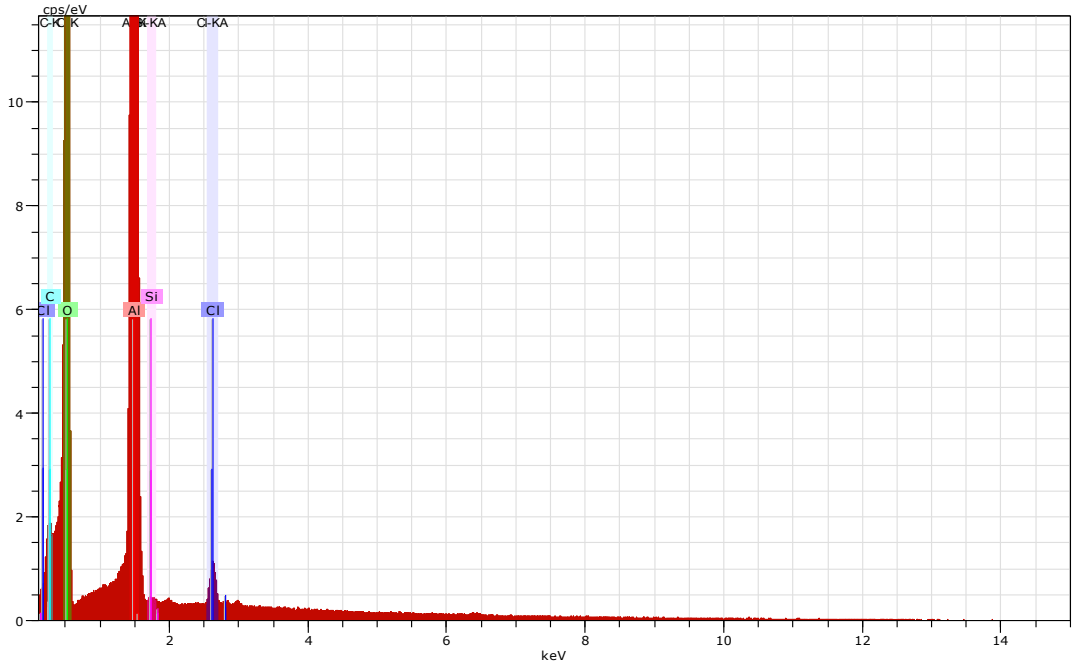

Figure 3-18 - EDX line spectrum of unmodified alumina aerogel (Ep1) collected at 15 keV with a spot size of 700 Å.

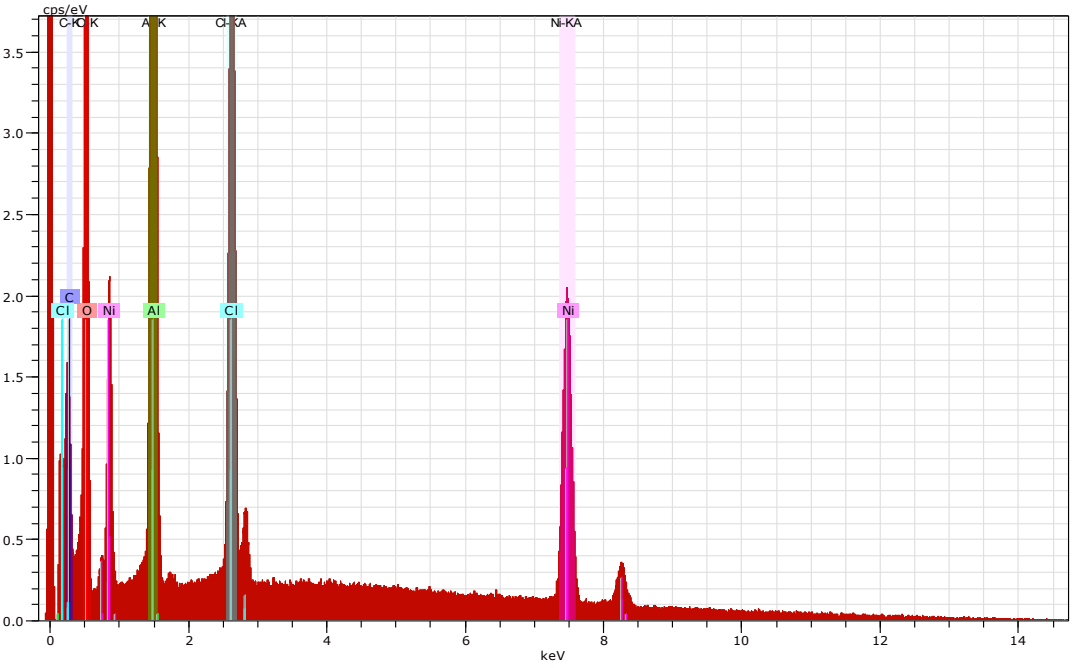

Figure 3-19 - EDX line spectrum of nickel-alumina aerogel prepared by direct addition (NEp2) collected at 15 keV with a spot size of 700 Å.

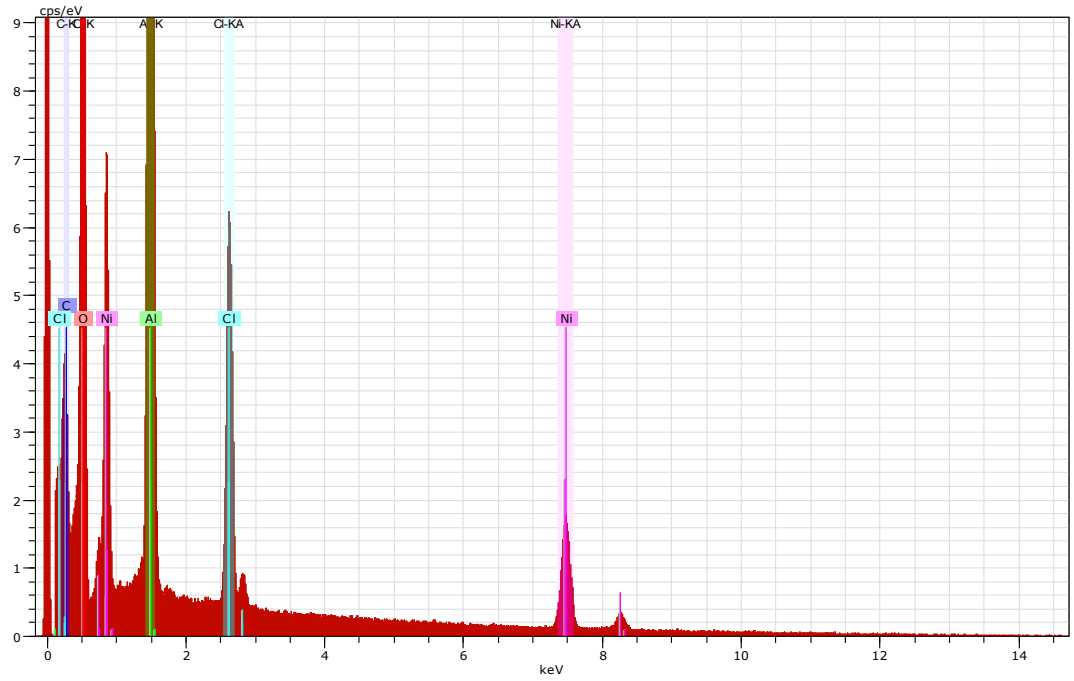

Figure 3-20 - EDX line spectrum of nickel-alumina aerogel prepared by solvent impregnation (NImp) collected at 15 keV with a spot size of 700 Å.

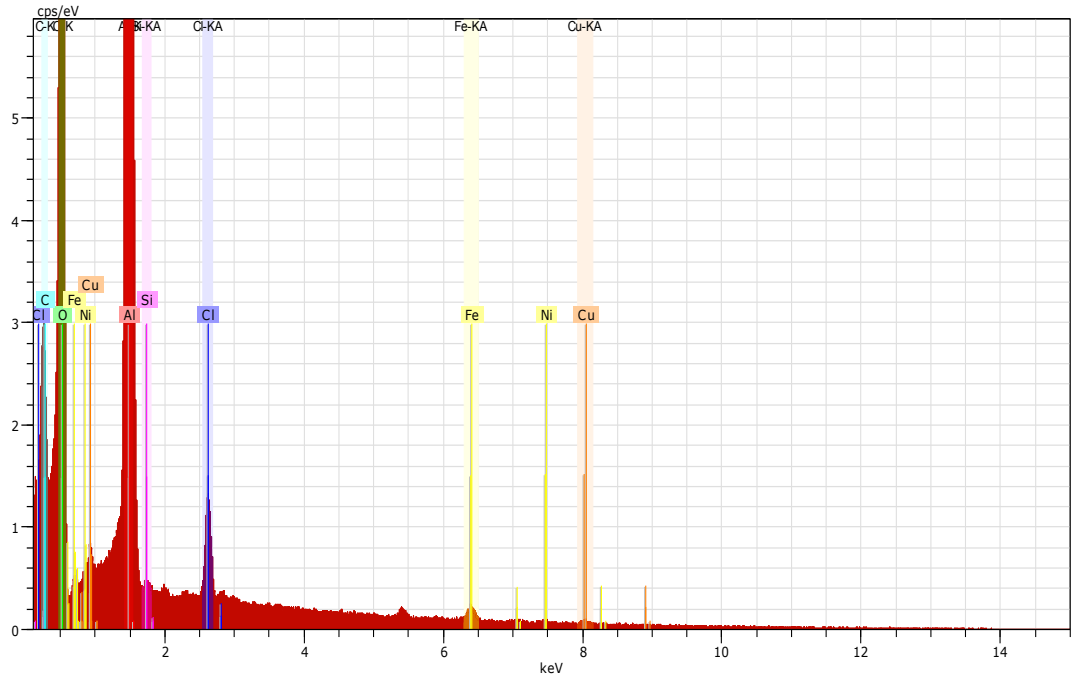

Figure 3-21 - EDX line spectrum of a low copper-content copper-alumina aerogel prepared by direct addition (CEp1) collected at 15 keV with a spot size of 700 Å.

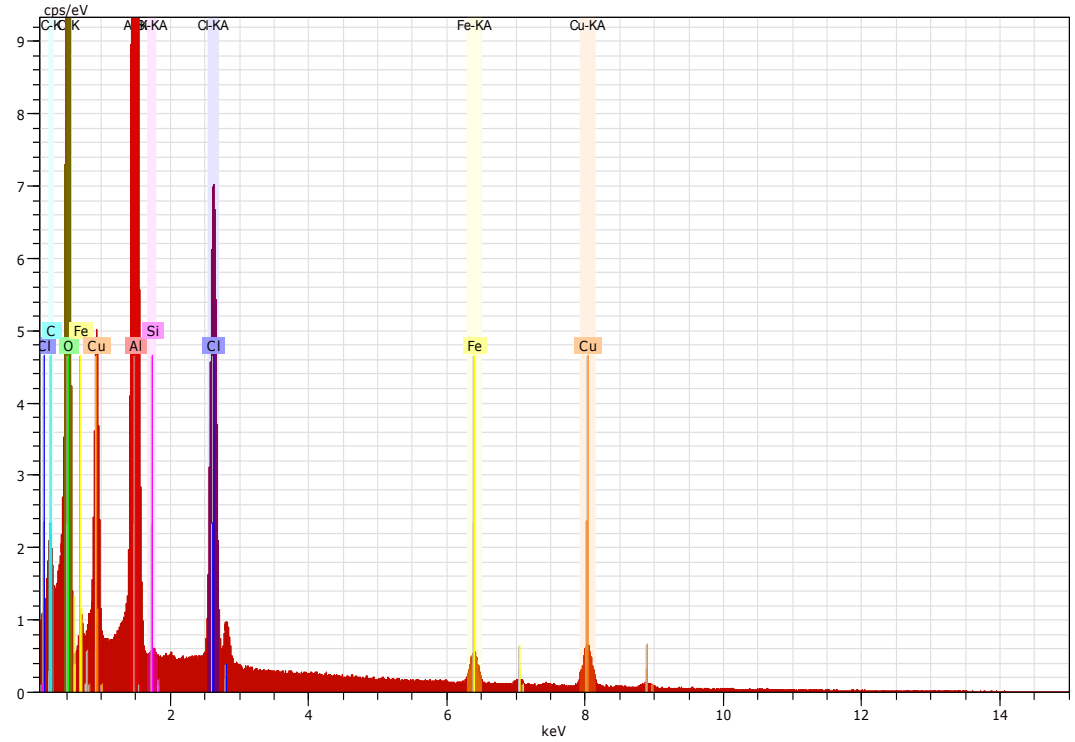

Figure 3-22 - EDX line spectrum of copper-alumina aerogel prepared by direct addition (CEp2) collected at 15 keV with a spot size of 700 Å.

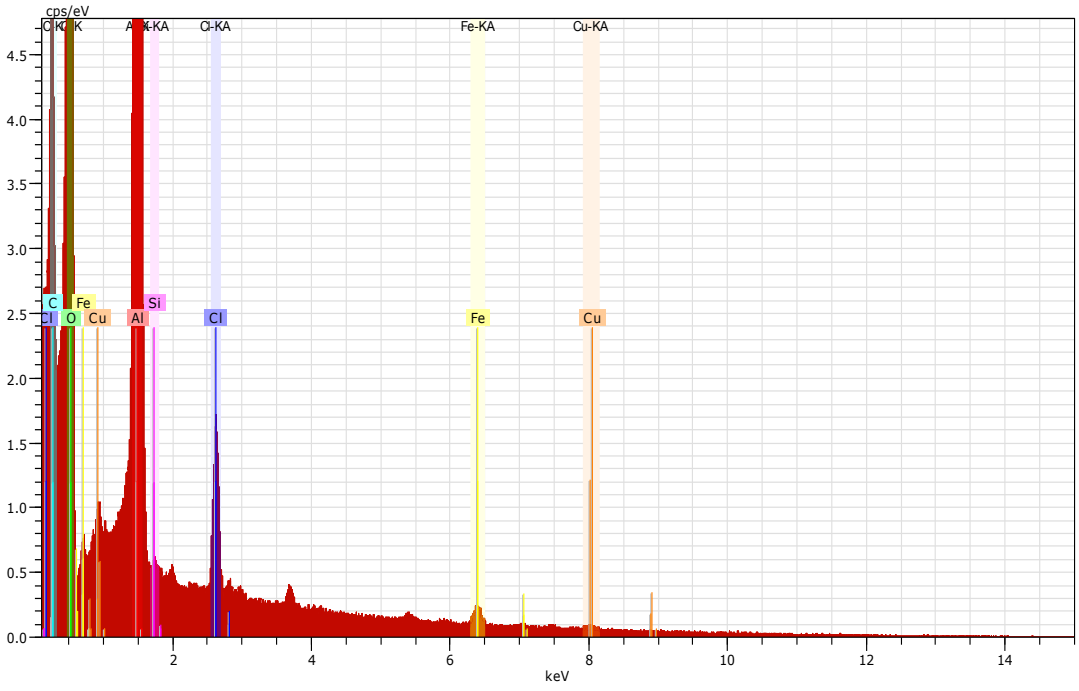

Figure 3-23 - EDX line spectrum of a low copper-content copper-alumina aerogel prepared by solvent impregnation (CImp-D) collected at 15 keV with a spot size of 700 Å.

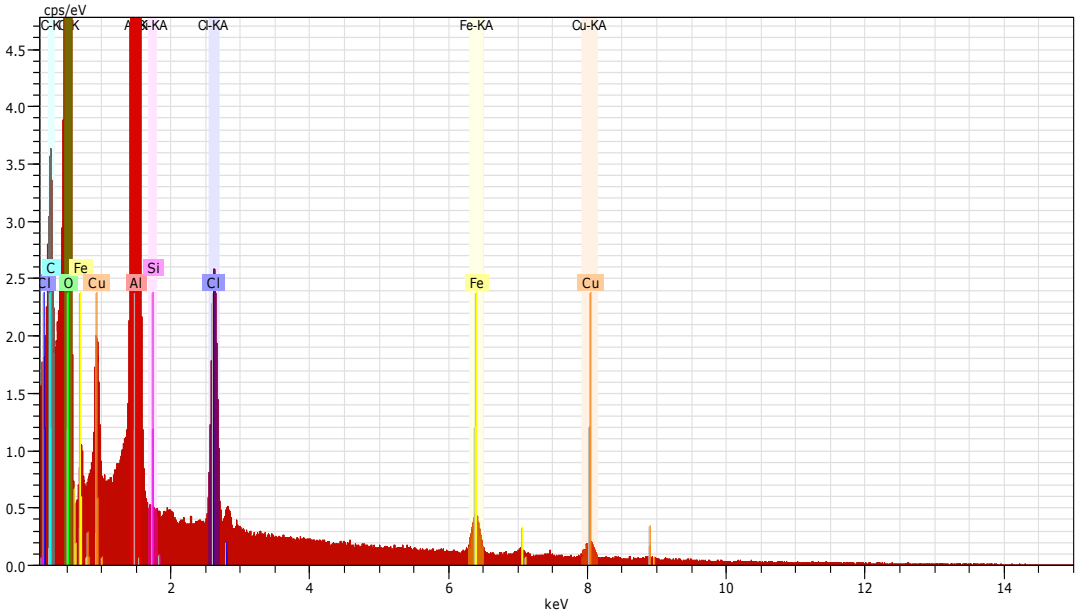

Figure 3-24 - EDX line spectrum of copper-alumina aerogel prepared by solvent impregnation (CImp) collected at 15 keV with a spot size of 700 Å.

EDX mapping studies of unmodified alumina aerogels (Fig 3-25) show an even distribution of aluminum and oxygen throughout the material as would be expected for amorphous alumina. Chlorine, likely in the form of chloride, is also evenly distributed throughout the material.

For nickel-alumina aerogels prepared by direct addition (Fig. 26) and solvent impregnation (Fig. 27), aluminum and oxygen are consistently present in the same locations. There are places where material is present in the SEM image where signal for neither aluminum or oxygen is present, but these areas may be dark due to the geometry between the detector and the sample. Nickel is consistently present throughout the materials, and its signal does not appear to change in intensity relative to changes in oxygen and aluminum density. This may be caused by a combination of effects from accelerating voltage and particle geometry. Figures 3-26 and 3-27 were gathered with an accelerating voltage of 15 keV, which is ideal for generating x-rays from nickel atoms

but is less efficient at generating x-rays from aluminum and oxygen. Combined with non-ideal particle geometry relative to the detector, this could cause the apparent shadows in aluminum and oxygen signal on the sides of some of the larger particles.

The copper-alumina samples did not did not suffer from the same geometry issues as the nickel-alumina samples, as the particles were arranged more uniformly in the copper-alumina sample. For the copper-alumina aerogels prepared by direct addition, both low copper-content (CEp1, Fig 3-28) and high copper-content (CEp2, Fig 3-29) as well as for the samples prepared by solvent impregnation, both the low (CImp-D, Fig. 3-30) and the high (CImp, Fig. 3-31) copper-content recipes, copper, aluminum and oxygen are present everywhere material is visible in the SEM image. For all of the recipes, copper is present at a lower apparent concentration than either aluminum or oxygen based on the relative signal intensities for these elements. These apparent relative abundances are consistent with the recipe used to prepare the material, which incorporates a relatively small amount of copper into an alumina sol gel by solvent impregnation.

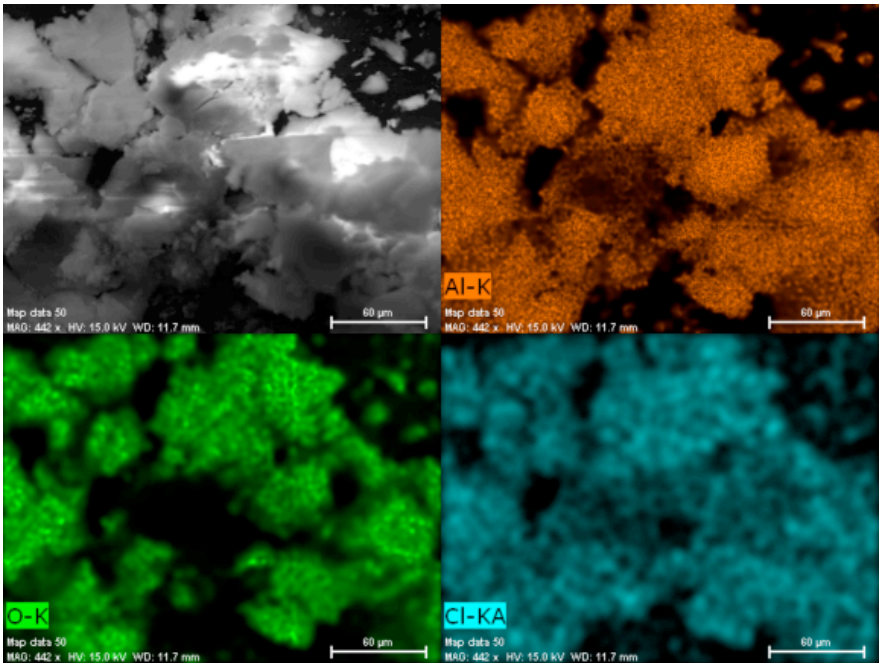

Figure 3-25 - EDX element mapping for an unmodified alumina aerogel (Ep1) collected at 15 keV with a spot size of 700 Å. Clockwise from the upper left, the images are: secondary electron (SEM), aluminum, oxygen, and chlorine.

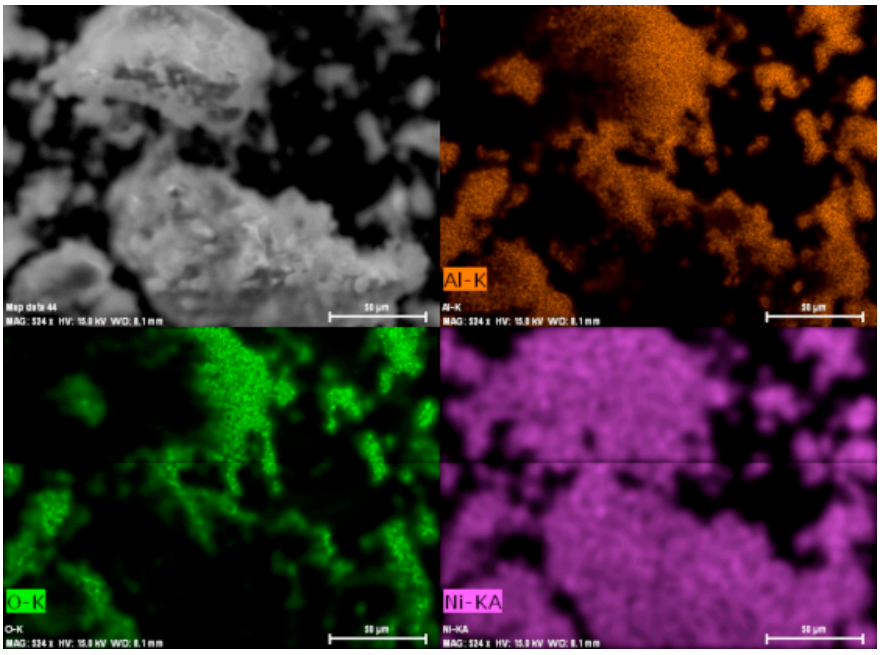

Figure 3-26 - EDX element mapping for nickel-alumina aerogel prepared by direct addition (NEp2) collected at 15 keV with a spot size of 700 Å. Clockwise from the upper left, the images are: secondary electron (SEM), aluminum, oxygen, and nickel.

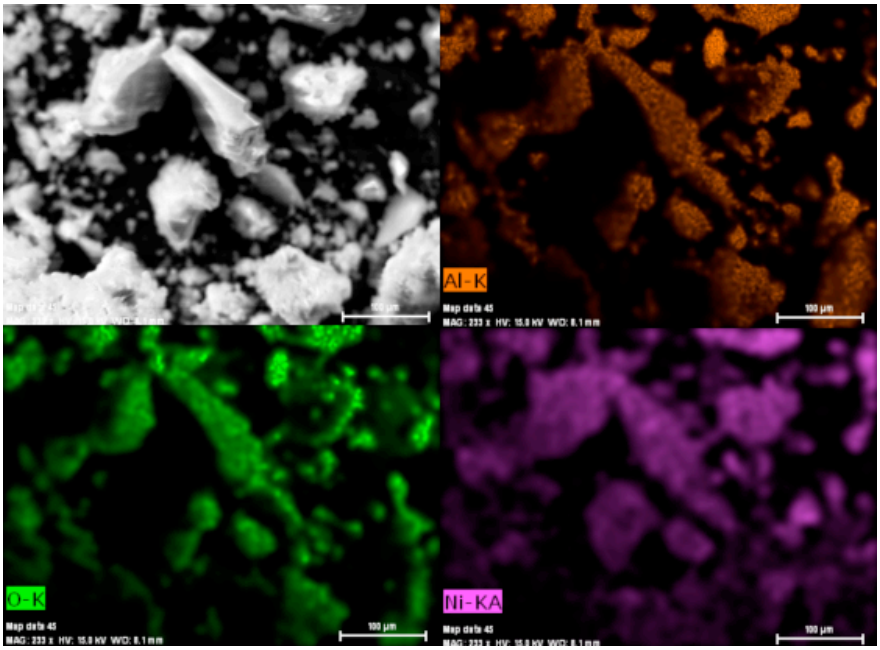

Figure 3-27 - EDX element mapping for nickel-alumina aerogel prepared by solvent impregnation (NImp) collected at 15 keV with a spot size of 700 Å. Clockwise from the upper left, the images are: secondary electron (SEM), aluminum, oxygen, and nickel.

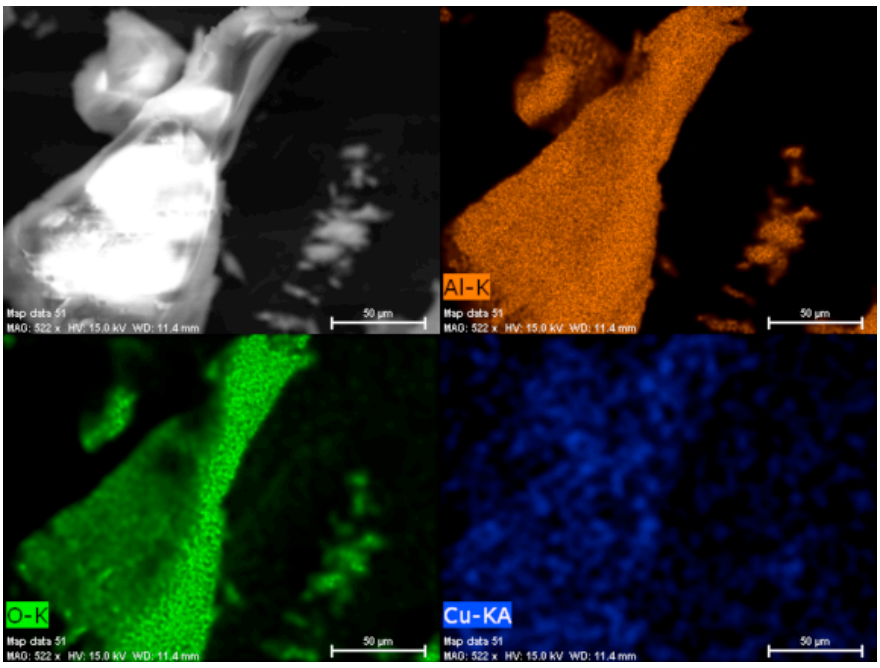

Figure 3-28 - EDX element mapping for a low copper-content copper-alumina aerogel prepared by direct addition (CEp1) collected at 15 keV with a spot size of 700 Å. Clockwise from the upper left, the images are: secondary electron (SEM), aluminum, oxygen, and copper.

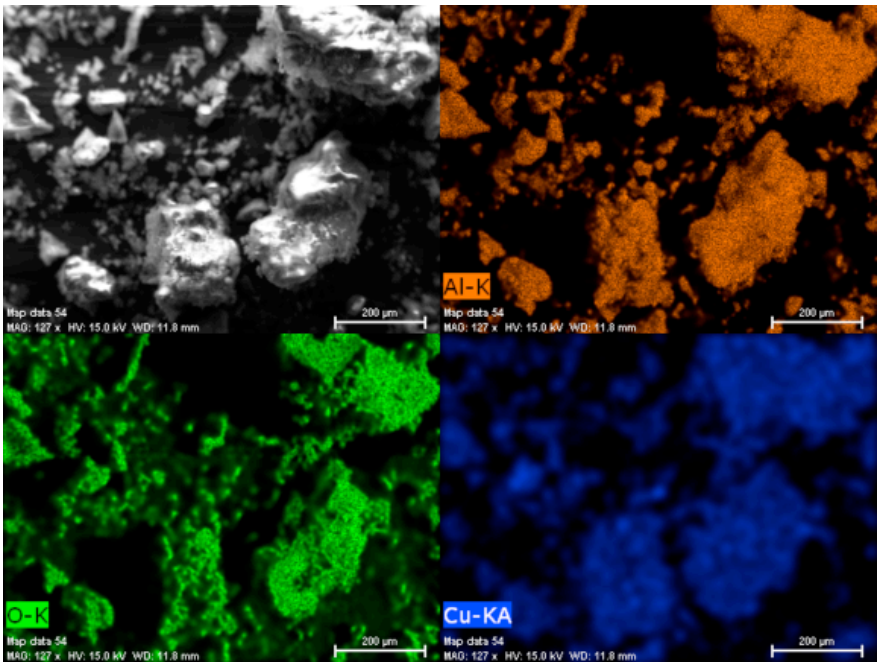

Figure 3-29 - EDX element mapping for copper-alumina aerogel prepared by direct addtion (CEp2) collected at 15 keV with a spot size of 700 Å. Clockwise from the upper left, the images are: secondary electron (SEM), aluminum, oxygen, and copper.

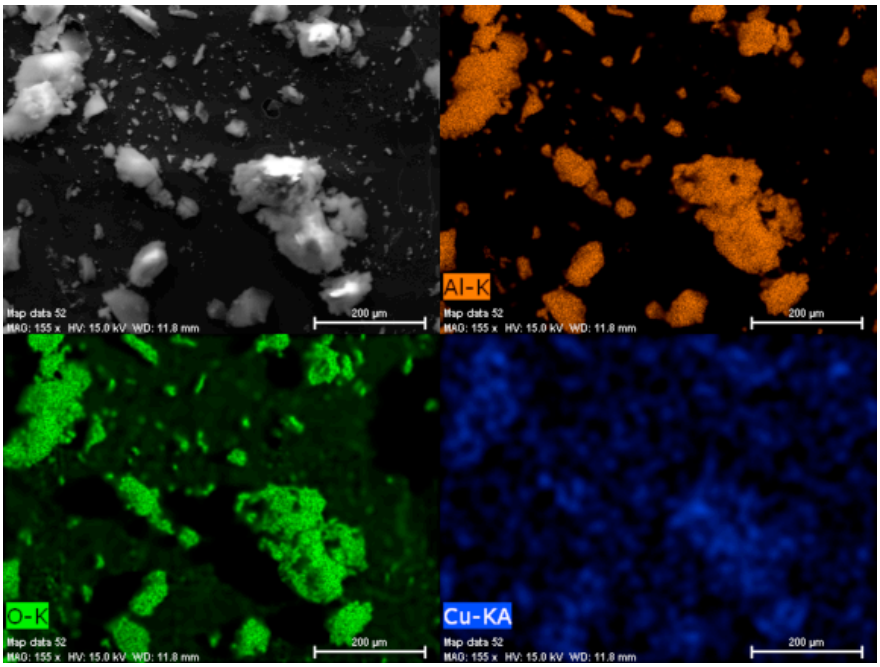

Figure 3-30 - EDX element mapping for a low copper-content copper-alumina aerogel prepared by solvent impregnation (CImp-D) collected at 15 keV with a spot size of 700 Å. Clockwise from the upper left, the images are: secondary electron (SEM), aluminum, oxygen, and copper.

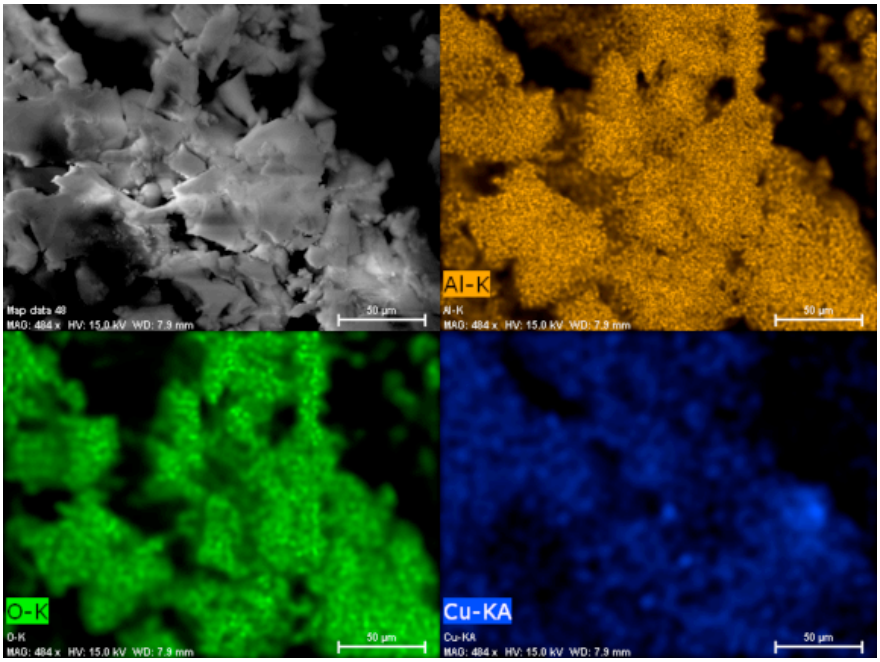

Figure 3-31 - EDX element mapping for copper-alumina aerogel prepared by solvent impregnation (CImp) collected at 15 keV with a spot size of 700 Å. Clockwise from the upper left, the images are: secondary electron (SEM), aluminum, oxygen, and copper.

References

[1] Janosovits, U., Ziegler, G.m Scharf, U.Wokaun, A. 1997. "Structural characterization of intermediate species during synthesis of Al_2O_3-aerogels. *J. Non-Cryst. Solids* 210, 1-13.

[2] Mizumisha, Y., Hori, M. 1995. "Alumina-silica aerogel catalysts prepared by two supercritical drying methods for methane combustion." *J. Mat. Sci.* 30, 1551-1555

[3] Baumann, T.F., Gash, A.E., Chinn, S.C., Sawvel, A.M., Maxwell, R.S. and Satcher, J.H. 2005. "Synthesis of high surface-are alumina aerogels without the use of alkoxide precursors." *Chem. Mater.* 17, 395-401

[4] Jellinek, M. H., Fankuchen, I. 1945. "X-ray diffraction examination of gamma alumina." *Ind. and Eng. Chem.* 37, 158-163.

[5] Bianchi, A. E., Plivelic, T. S., Punte, G., Torriani, I. L. 2008. "Probing the structure of nanograined CuO powders." *J. Mater. Sci.* 43, 3704-3712.

[6] Hao, Z., Zhu, Q., Lei, Z., Li, H. 2008. "CH_4-CO_2 reforming over Ni/Al_2O_3 aerogel catalysts in a fluidized bed reactor." *Powder Technol.* 182, 474-479

[7] Kim, H.-J., Suh, D. J., Park, T.-J., Kim, K.-L. 2000. "Effect of metal particle size on coking during CO_2 reforming of CH_4 over Ni-alumina aerogel catalysts." *Appl. Catal.* 197, 191-200.

[8] Krompiec, S., Mrowiec-Bialon, J., Skutil, K., Dukowitz, A., Pajak, L., Jarzebski, A.B., 2004. "Nickel-alumina composite aerogel catalysts with a high nickel load: a novel fast sol-gel synthesis procedure and screening of catalytic properties." *J. Non-Cryst. Solids* 315, 297-303

Catalytic Characterization Experimental

Characterization of Solvent

In order to determine whether the alumina and nickel-alumina aerogels were catalyzing reactions of the ethanol solvent during supercritical extraction on the hot press, a program was designed to collect the solvent after the run was complete. In order to not release the supercritical solvent, the restraining force was not reduced at high temperature and pressure. This allowed liquid solvent to be collected after the hot press cooled and opened. The precursor recipes used for this study all utilized an ethanol solvent. The recipes used were unmodified alumina (Ep1), nickel-alumina by direct addition (NEp2) and nickel-alumina by solvent impregnation (NImp). Each of these samples underwent a single solvent exchange prior to processing in the hot press

The parameters for this program were identical to those of program 6F*45 from Table 2-2 with two exceptions: (1) the force was set to remain at a constant 200 kN, and (2) a dwell time of 90 minutes at high temperature and pressure was included to keep the length of the high temperature and pressure conditions consistent with program 6F*45. The addition of the dwell time replaced the time that was previously taken up by reducing the force. Once the cooled hydraulic press opened, the liquid samples were withdrawn using Pasteur pipettes to minimize the collection of aerogel particulates. The samples were stored in a refrigerator at 4 ºC when not in use. Ethanol blanks were run in the stainless steel mold in the absence of sol-gel samples to control for non-aerogel catalytic interactions in the system.

Since the possibility of aerogel nanoparticles as well as water and nonvolatile

compounds in the liquid sample could not be eliminated, the samples were examined by GC-MS headspace analysis rather than by a liquid injection. The samples were analyzed on an Agilent 6890 GC/MS unit with an autosampler and an Agilent 190915-433 HP-SMS 5% phenyl methyl siloxane capillary column measuring 30 m in length, using He as the carrier gas. The mass spectrometer was set to detect fragments with m/z ratios between 10 and 500. A quantity of 3.0 μL of headspace gas was withdrawn over several drops of the sample and injected onto the column in a splitless injection. In order to increase the presence of less volatile species in the headspace the samples were heated to approximately 37 ºC immediately prior to injection using human body heat. Since the injected sample was gaseous at low temperature, the temperature profile was held constant at 40 ºC for a total of 5 min.

Standards of likely components of the sample were also analyzed via headspace GC-MS. These standards included ethanol (Fisher, ≥99.8%), methanol (Fisher, 97%), acetone (Fisher, 97%), diethyl ether (Sigma-Aldrich, 99%), ethyl acetate (Sigma-Aldrich, 99.8%), ethyl propionate (Sigma-Aldrich, 99.7%) and 2-butanone (Sigma-Aldrich, 99.7%).

Characterization of Exhaust Cleaning Activity

Catalytic activity for CO, NO and hydrocarbon conversion was tested on a test bed designed by students Max Becton and Justin Rodriguez from the Mechanical Engineering department at Union College. The apparatus consists of a reactor tube 9 cm in length by 4 cm in diameter that contains the aerogel sample. Heated gas (500 ºC) was passed through the chamber with a space velocity range of 5-10 s^{-1} and the reactor was

heated to maintain a constant temperature of 500 ºC. A BAR 97 emissions blend 32 gas canister, containing 200 ppm C_3H_8, 0.5% CO, 6.0% CO_2 and 30 ppm NO, was used to simulate automobile exhaust. This gas mixture was passed over either an aerogel powder or a cordierite plug coated with an aerogel film and the composition of the gas exiting the reactor was monitored. An EMS 5002 5 Gas Analyzer was used to determine the concentrations of hydrocarbons, CO_2, O_2, CO and NO in the post-reactor gas in order to determine the extent of conversion. For comparison, two control conditions were utilized. First, a high-temperature (500ºC) run using compressed air rather than the exhaust blend was used to control for emissions from the apparatus and aerogel material. The second control was a run at room temperature with the exhaust blend and was used to determine the composition of the relatively unaltered emissions blend passing through the sample.

Results and Discussion: Catalytic Characterization

GC-MS and Catalysis

The composition of the recondensed solvent ethanol was investigated by GC-MS to determine the identity the compound(s) giving rise to a butterscotch-like odor emanating from several aerogel samples. The hypothesis was that the ethanol was undergoing reactions to form esters on the surface of the aerogel, during RSCE processing. This seemed plausible because the conditions during extraction were not dissimilar to those used during several known ethanol processing reactions,[1,2] and because the alumina and nickel-alumina aerogels are intended to be catalytic by their design. Jain et al. discuss the mechanism for formation of diethyl ether over acid sites on an alumina catalyst,[1] whereas Gomez et al. describe the formation of 1,1-diethoxyethane from bioethanol over acidic alumina catalyst.[2]

GC-MS headspace analysis revealed that reactions were taking place during the extraction process and that ethers were the main products of these reactions. Peaks were identified on the basis of their fragmentation patterns, as well as by comparing retention time to a standard when standards were available. The fragmentation patterns were interpreted manually, with the use of the NIST mass spectroscopy library as a guide. Diethyl ether was the reaction product that gave the largest chromatographic peak, as seen below in Figure 5-1. Other products included methyl ethyl ether, acetone and diethyl acetal. These products were common to both alumina and nickel alumina aerogels in similar proportions, as seen in Figures 5-2 and 5-3, which are from solvent samples that were heated over NEp2 and NImp1 sol gels, respectively.

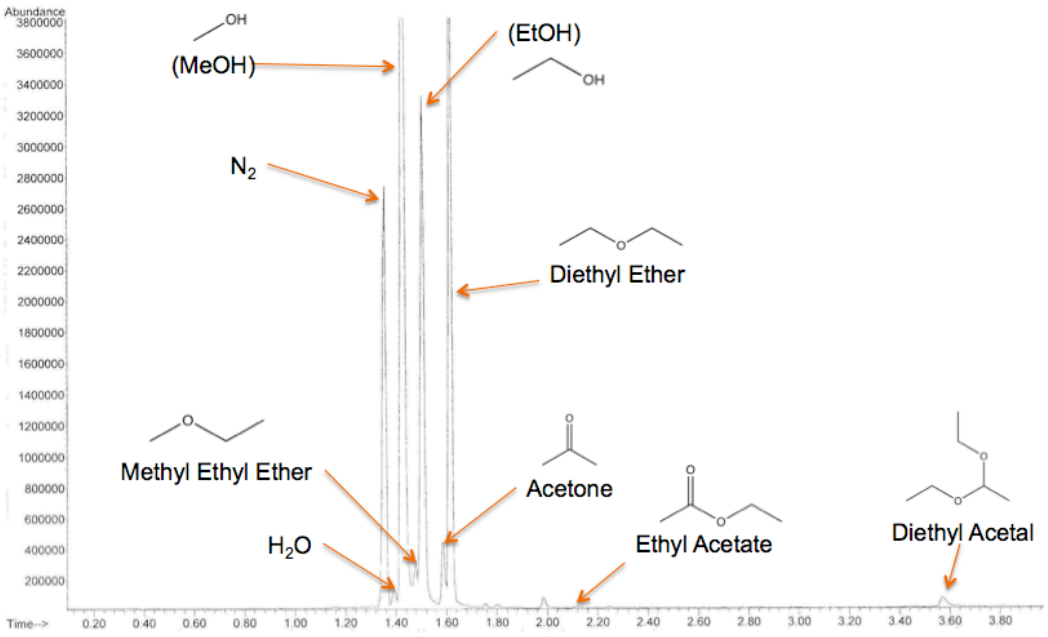

Figure 5-1: Gas chromatogram of headspace over sample of ethanol that underwent supercritical conditions. This sample was processed in the hot press with the alumina Ep1 recipe. The sample was injected by splitless injection, no solvent delay, m/z ratios from 10-500.

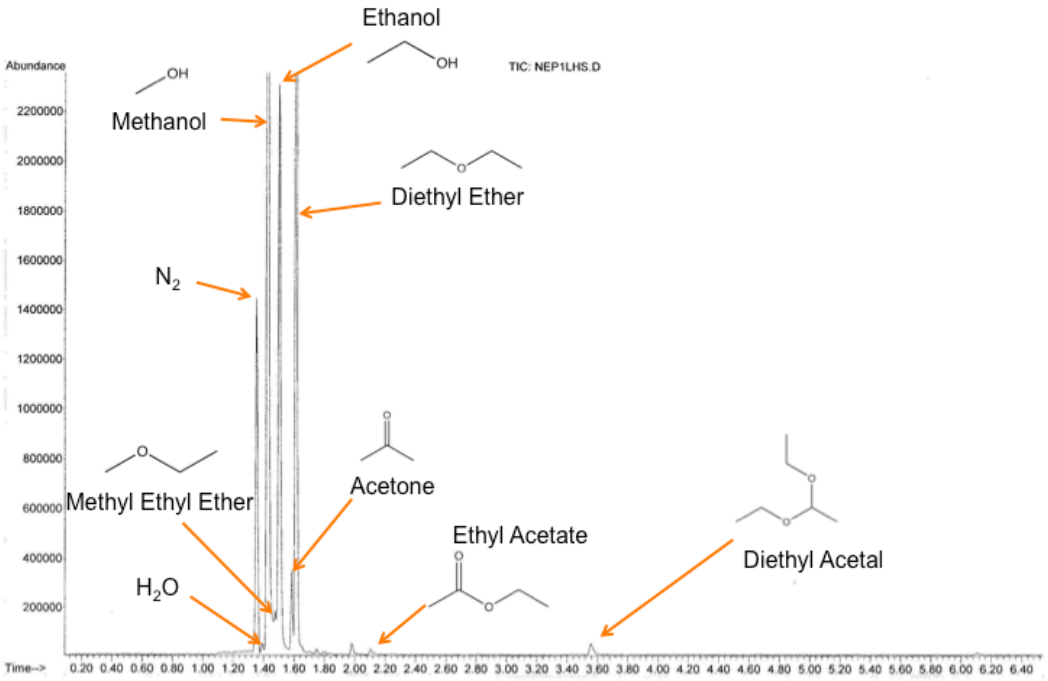

Figure 5-2: Gas chromatogram of headspace over sample of ethanol that underwent supercritical conditions. This sample was processed in the hot press with the alumina NEp2 recipe. The sample was injected by splitless injection, no solvent delay, m/z ratios from 10-500.

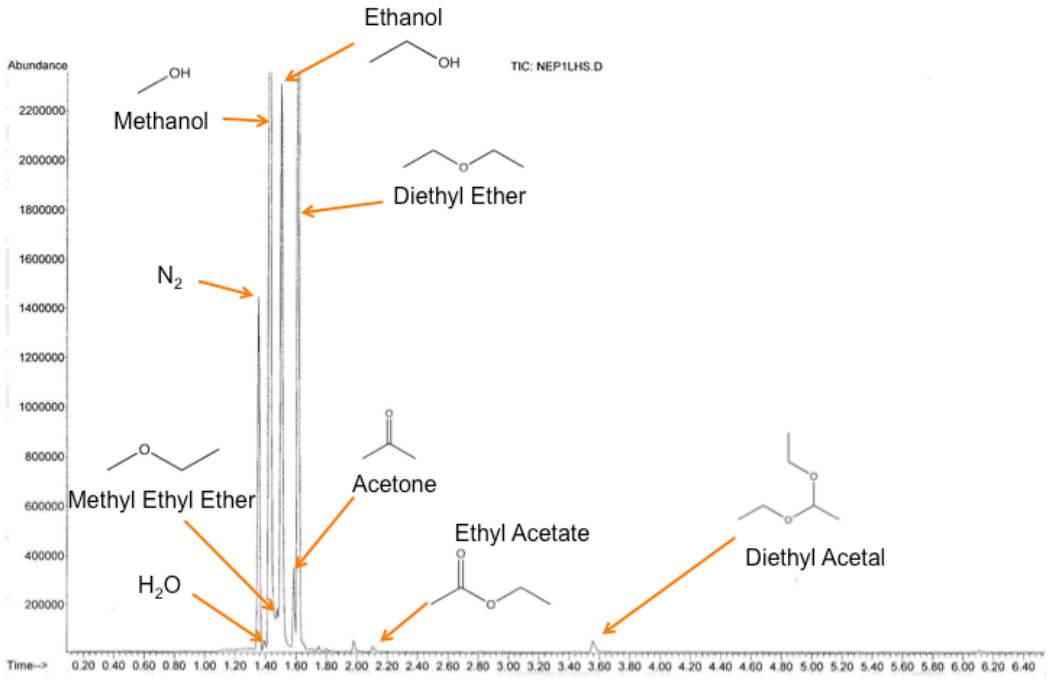

Figure 5-3: Gas chromatogram of headspace over sample of ethanol that underwent supercritical conditions. This sample was processed in the hot press with the alumina NImp1 recipe. The sample was injected by splitless injection, no solvent delay, m/z ratios from 10-500.

Ethyl acetate was seen as a significant peak in both nickel alumina samples tested, but was only present at trace level in the unmodified alumina sample. The ethyl acetate peaks for direct addition and solvent exchange impregnation of nickel can be seen in Figures 5-2 and 5-3. This would seem to implicate the involvement of nickel in the reaction producing ethyl acetate.

The methanol and N_2 peaks are artifacts of the sample injection process: some air is injected with any headspace sample and the injection syringe was washed with methanol during the injection procedure. Peaks attributable to both methanol and N_2 are observed following an injection of an ambient air blank. The water peak comes primarily from ambient humidity.

Without the use of internal standards it is impossible to quantitatively compare

sample composition between injections. Internal standards are difficult to employ in headspace analysis as the volatility of the standard must be taken into account, and the composition of the headspace relies on the volatility and molar ratios of the components of the liquid phase.

Catalytic Converter Test Bed

In order to control for interactions between the emissions blend and the test bed, several control runs were performed, the results of which can be found in Table 5-1. The emissions blend itself contains 200 ppm C_3H_8, 0.5% CO, 6.0% CO_2, and 300 ppm NO, so these readings should show up in the cold emissions test, in which the emissions blend was passed through the empty test bed at room temperature. For each test, the readings closely match up with the predicted values for this control. Oxygen is also detected, suggesting the possibility of a small air leak into the line from the test bed's surroundings.

Identical runs were performed on Michael Bono's MB-14 alumina aerogel samples, and the results (Table 5-2) likely indicate an air leak into the testing line. The oxygen content was reported at around 5% for each of the runs, approximately ten times the amount indicated for the emissions blend.

Table 5-1: Contents of Emissions Blend Run Through Empty Test Bed

Test Type	hydrocarbons (ppm)	% O2	NO (ppm)	% CO2	% CO
Emissions blend	200	0	300	6.0	0.50
500 ºC air and emissions	196	1.38	285	5.8	0.46
20 ºC air and emissions	174	3.76	241	5.0	0.41
20 ºC emissions	196	0.13	303	6.0	0.50

Table 5-2: Contents of Emissions Blend Run through MB-14 Alumina Aerogel and Percent Error Relative to Emissions Blend with 0.17% Air

	500 ºC air and emissions	% error	20 ºC air and emissions	% error	20 ºC emissions	% error
Hydrocarbons (ppm)	156	22	154	23	154	23
% O2	4.13	-	5.61	-	5.38	-
NO (ppm)	234	22	217	28	221	26
% CO2	4.9	18	4.5	25	4.5	25
% CO	0.38	24	0.37	26	0.38	24

Since air is around 20.9% oxygen by volume, this would correspond to a leak where the contents of the line were 25% air by volume. This would be predicted to cause a 25% decrease in the other analytes present, which is observed for each of the trials with the exception of the percent CO_2 in the 500 ºC trial. The presence of this leak makes it impossible to accurately determine whether or not the aerogel powder was effective at altering the composition of the emissions blend for these runs. The catalytic effectiveness would need to be relatively small to be completely masked by the air leak.

The aerogel powder used in these runs was initially cloudy white in appearance, but took on a grey, soot-like color after use in the test bed. Neither heating at 180 ºC, desiccation nor degassing under vacuum resulted in regenerating the original appearance of the material.

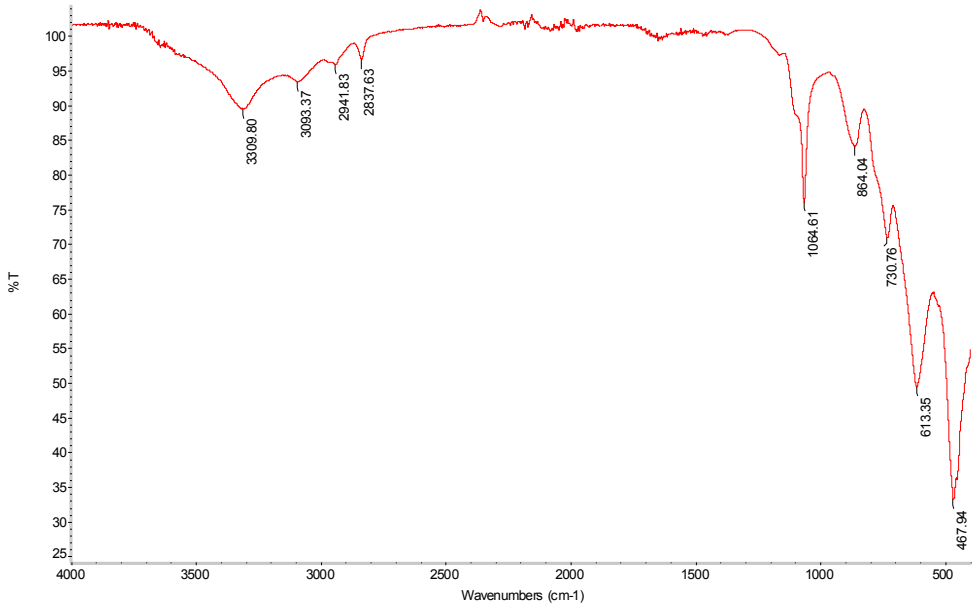

Figure 5-4 - FTIR spectrum of MB-14 alumina aerogel prior to exposure to test bed conditions, taken using an ATR attachment with a resolution of 4 cm^{-1} averaged over 32 scans.

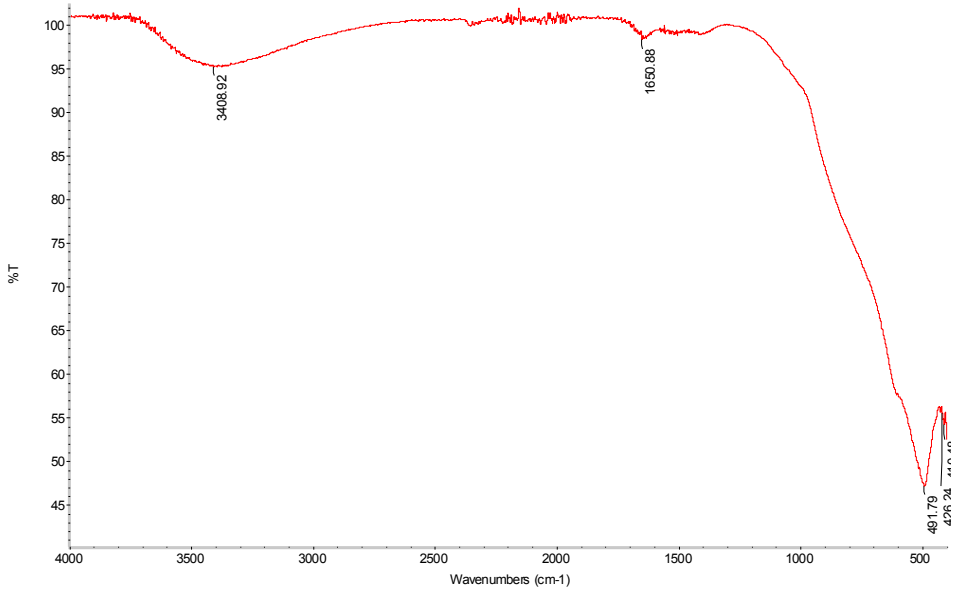

Figure 5-5 - FTIR spectrum of MB-14 alumina aerogel after exposure to test bed conditions, taken using an ATR attachment with a resolution of 4 cm^{-1} averaged over 32 scans.

Heating, desiccating and degassing under vacuum were attempted in order to remove adsorbed species on the surface of the material, which may have led to the change in the samples' appearance. The IR spectra of these aerogels also changed considerably from before the test-bed experiment, as seen in Figures 5-4 and 5-5. The sharp detail of the spectrum in Figure 5-4 is washed out in Figure 5-5, possibly due to adsorbed species masking the sharp absorption bands of the underlying aerogel material. Heating, desiccation and degassing under vacuum reduced the intensity of the broad -OH peak around 3300 cm^{-1}, but did not eliminate it or regenerate any of the fine detail present in the pre-test bed sample.

References

[1] Jain, R. J.; Pillai, C. N. 1967. "Catalytic dehydration of alcohols over alumina mechanism of ether formation." *Journal of Catalysis* 9, 322-330.

[2] Gomez, M. F., Arrúa, L.A.; Abello, M.C. 2001. "Synthesis of 1,1 diethoxyethane from bioethanol. Influence of catalyst acidity." *React. Catal. Lett.* 73, 143-149.

Conclusions

Rapid supercritical extraction can be used to prepare high quality alumina-based aerogels with surface areas in the 550 - 800 m^2/g range and bulk densities between 0.05 - 0.15 g/mL. These aerogels are nanoporous as confirmed by nitrogen porosimetry and SEM characterization, and contain boehmite microcrystalline phases as demonstrated using powder XRD. The microcrystalline phases are more pronounced in unmodified alumina aerogels than in nickel-alumina or copper alumina aerogels, possibly due to the secondary metals interrupting the formation of the boehmite crystallites.

The addition of nickel decreases the specific surface area of samples relative to their unmodified alumina counterparts, though this effect can be mitigated using a solvent impregnation method to incorporate nickel rather than direct addition. The use of water in the reaction solvent helps to dissolve the aluminum chloride, but is detrimental to the surface area and increases the bulk density of samples relative to their pure alcohol counterparts.

The use of EDX spectroscopy demonstrates that nickel and copper evenly distribute throughout the aerogel material in both the solvent impregnation and direct addition methods. EDX line spectra indicate that chlorine and silica are common contaminants of my samples, and that copper-alumina aerogels incorporate iron during processing.

Layers of aerogel material can be deposited inside cordierite channels using a dip-coating method without treating or modifying the surface of the cordierite. Cordierite samples that have been dip-coated can be processed in the same way as a normal aerogel sample, including the use of solvent exchanges and RSCE.

Alumina aerogels demonstrate catalytic activity under RSCE conditions with ethanol, forming diethyl ether and diethyl acetal through dehydration of ethanol. Acetone, methyl ethyl ether and ethyl acetate are also formed under RSCE conditions through unknown mechanisms.

Alumina aerogel samples prepared in 200# by Michael Bono irreversibly change after being used in the catalytic test bed, becoming dark grey in color rather than their original white. This change in color coincides with a change in the IR spectrum of the sample, which loses the fine details of the alumina absorption bands. The original color and IR spectrum cannot be regenerated using desiccation, heating or degassing under vacuum.

Future Work

Work continuing in this area should focus on determining the catalytic efficiency of alumina-based aerogels for exhaust-processing reactions. If any catalysis is observed, these measurements should be repeated over time to determine the useful lifetime of an aerogel-based catalytic converter. Correlating catalytic efficiency and effective lifetime with physical properties of the aerogel material will be necessary in order to optimize the aerogel material for automotive catalysis.

In the event that alumina-based aerogels do not have favorable effective lifetimes as automotive catalysts, incorporating silica into the material or replacing the alumina phase with silica or organically modified silica may help to provide additional heat and water resistance to the material.

If copper-alumina aerogels prepared by RSCE have favorable catalytic properties, work should be done to characterize the interaction between copper and iron that occurs in the hydraulic hot press. Currently, iron appears to be incorporating into the aerogel material at levels comparable to the copper present.